

# Differences in physical properties of coronal bright points and their ALMA counterparts within and outside coronal holes

F. Matković<sup>1</sup>, R. Brajša<sup>1</sup>, M. Temmer<sup>2</sup>, S. G. Heinemann<sup>3</sup>, H.-G. Ludwig<sup>4</sup>, S. H. Saar<sup>5</sup>, C. L. Selhorst<sup>6</sup>, I. Skokić<sup>1</sup>, and D. Sudar<sup>1</sup>

<sup>1</sup> Hvar Observatory, Faculty of Geodesy, University of Zagreb, Kačićeva 26, 10000 Zagreb, Croatia

<sup>2</sup> University of Graz, Institute of Physics, Universitätsplatz 5, 8010 Graz, Austria

<sup>3</sup> Max Planck Institute for Solar System Research, Justus-von-Liebig-Weg 3, 37077 Göttingen, Germany

<sup>4</sup> Landessternwarte, Zentrum für Astronomie der Universität Heidelberg, Königstuhl 12, 69117 Heidelberg, Germany

<sup>5</sup> Harvard-Smithsonian Center for Astrophysics, 60 Garden Street, Cambridge, MA 02138, USA

<sup>6</sup> NAT - Núcleo de Astrofísica, Universidade Cruzeiro do Sul/Universidade Cidade de São Paulo, São Paulo, SP, Brazil

Received date, accepted date

## ABSTRACT

**Aims.** This study investigates and compares the physical properties, such as intensity and size, of coronal bright points (CBPs) inside and outside of coronal holes (CHs) using Atacama Large Millimeter/submillimeter Array (ALMA) and Solar Dynamics Observatory (SDO) observations.

**Methods.** CBPs were analyzed using single-dish ALMA Band 6 observations, combined with SDO EUV 193Å filtergrams and Helioseismic and Magnetic Imager (HMI) magnetograms. From EUV images CH boundaries were extracted using Collection of Analysis Tools for Coronal Holes (CATCH) and CBPs were identified in EUV and magnetogram data and in ALMA data. Measurements of CBP intensity and sizes in both ALMA Band 6 and SDO EUV images were conducted for CBPs within CH boundaries and quiet Sun regions. Two equal size CBP samples, one inside and the other outside CHs, were randomly chosen and statistical analysis was conducted. The statistical analysis was repeated 200 times using a bootstrap technique to eliminate results based on pure coincidence.

**Results.** Boundaries of five selected CHs were extracted using CATCH and their physical properties were obtained. Statistical analysis of the measured physical CBP properties using two different methods resulted in lower average intensity for CBPs within the boundaries of all five CHs. Depending on the individual CBP sample size and the observed CH, the difference in intensity between the CBPs inside and outside CHs ranged between  $2\sigma$  and  $6\sigma$ , showing statistically significant difference between those two CBP groups. We also obtained CBP sizes (diameter) and areas, where CBPs within the CH boundaries showed lower values of the measured sizes and areas, with the observed difference between the CBPs inside and outside CHs between  $1\sigma$  and  $5\sigma$ , indicating that CBP sizes and areas are also significantly different for the two CBP groups. We also found that, in comparison to SDO data, the measured ALMA properties show a smaller difference in the observed properties between the CBPs inside and outside CH in the majority of the cases, possibly because of the modest spatial resolution of the ALMA images.

**Conclusions.** Based on the extracted physical properties, all five selected CHs show a good agreement with the average CH properties found at the time of the solar minimum. Moreover, we conclude that larger CHs in general tend to contain larger numbers of CBPs within their boundaries. Given the measured physical properties of CBPs, we find that the CBPs inside CHs are on average less bright but also smaller in comparison to those outside of CHs. These results lead to a conclusion that the specific physical conditions and properties of the local CH region around a CBP could limit the maximum achievable intensity (temperature) and size of a CBP. The need for interferometric ALMA data is also emphasized to get more precise physical CBP property measurements at chromospheric heights.

**Key words.** Sun: coronal bright point – Sun: corona – Sun: chromosphere – Sun: radio radiation – Sun: EUV radiation

## 1. Introduction

Coronal bright points (CBPs) are one of the most frequent activity phenomenon in the solar atmosphere. They consist of low-corona small-scale plasma loops that connect two magnetic flux concentrations of opposite polarities in the photosphere (Madjarska 2019). Reale (2014) gives an insight into the nature of coronal loops being magnetic flux tubes with hot and dense confined plasma, where the CBPs occupy the low end of the size spectrum of coronal loops.

CBPs can be found in active regions, quiet Sun regions and within CHs (Madjarska 2019). In this study we only focus on CBPs in the quiet Sun regions and within CHs. Quiet Sun is regarded as the region with a diffuse plasma (at modest spatial

resolutions) devoid of sunspots and active regions (Bellot Rubio and Orozco Suárez 2019, Del Zanna and Mason 2018). At coronal heights, the temperature of the quiet Sun is found to be about 1 MK, or even more (Del Zanna and Mason 2018), and the electron density is found to be higher than  $4 \times 10^8 \text{ cm}^{-3}$  (Dere 2020). The quiet Sun regions have mixed-polarity magnetic field and are spattered with small bipolar regions that could give rise to CBPs ((Del Zanna and Mason 2018). CHs are the least active regions of the Sun that appear as dark structures in extreme-ultraviolet (EUV) and X-rays due to the cooler and less dense plasma than in the surrounding regions (Cranmer 2009). Using six coronal EUV filters from the Atmospheric Imaging Assembly (AIA) onboard of the Solar Dynamics Observatory (SDO), Heinemann et al. (2021a) found the average temperature of CHs

to be  $0.94 \pm 0.18$  MK and a mean electron density of  $(2.4 \pm 0.7) \times 10^8 \text{ cm}^{-3}$ . Even though CHs are known for the abundance of open magnetic field of a certain polarity, they still have regions of mixed-polarity magnetic field that enable CBP formation (Wiegelmann et al. 2005).

Mou et al. (2016) found that about half of the CBPs are related to newly emerging magnetic flux regions called ephemeral regions (Harvey et al. 1975), while others are related to encounters of converging magnetic flux. This is different than the older studies done by Harvey (1984) and Harvey et al. (1994) who found that 70% - 80% of CBPs were associated with the chance encounter of network flux and only 20% - 30% were related to newly emerging bipolar fluxes. Another older study done by Harvey (1985), who observed He I 10830 Å "dark points", known to be a counterpart of CBPs, and their associated magnetic bipoles, reported that 1/3 of the dark points were associated with ephemeral regions, with at least 2/3 being the result of the chance encounter of existing opposite polarities. The author also found that CBPs are driven by magnetic reconnection in the solar corona and that the flux chance encounter is the mechanism for the flux removal in the quiet Sun.

CBPs are also known to have an enhanced emission in the EUV and X-ray spectrum. They were first discovered in X-rays in 1969 in a series of rocket flights and were named X-ray bright points (XBPs) due to their point-like X-ray feature (Vaiana et al. 1970). In X-ray observations analyzed by Golub et al. (1977), the size (diameter) of compact X-ray CBP features ranged between 20" and 30", with a bright core of 5"-10" in diameter.

The first EUV CBP observations were analyzed by Habbal and Withbroe (1981) using Harvard EUV experiment on Skylab/ATM (Golub and Pasachoff 2010), showing that CBPs are composed of magnetic loops rooted in the chromosphere. They also found that CBP plasma heating occurs at coronal heights and is carried to the chromosphere by thermal conduction. Habbal et al. (1990) used spectroheliograms from the Harvard EUV experiment on Skylab/ATM to compare morphological structure and emission variations of CBPs in CHs and outside them in the quiet Sun region. These authors found that short-time variations in spectral lines were not always found to be co-spatial suggesting that CBPs are composed of loops of various sizes and temperatures. Additionally, quiet Sun and CH CBPs are found to range from 10" to 40" in diameter in both CH and the quiet Sun region and no difference between those CBPs related to the properties of the observed region was found. Another work done by Habbal and Grace (1991) using similar data showed that depending on the associated magnetic field strength, some CBPs could be composed of plasma loops that cannot reach coronal temperatures. Both previous works reported that the CBP formation and existence are independent of the overlying background coronal magnetic structure, but not a CBP evolution.

More CBP size measurements were conducted in recent years, and based on the full lifetime evolution of CBPs done by Mou et al. (2018) using SDO EUV data, CBPs that formed from magnetic flux emergence were initially only 5" in diameter and they reached a maximum size of up to ~60". The value of 60" as a maximum CBP size is used as a size limit when considering CBPs in most of the studies, but there are rare exceptions of CBPs going even up to ~100" in diameter (Madjarska et al. 2018). Based on the obtained results, we can say that a value between 5" and 60" could be considered as typical CBP sizes, as it is considered in the present paper.

On the other hand, the motions of CBPs in EUV data obtained by Solar and Heliospheric Observatory (SOHO) Extreme ultraviolet Imaging Telescope (EIT) and SDO AIA were used

as tracers to study solar differential rotation with great precision (Brajša et al. 2002; Wöhl et al. 2010; Sudar et al. 2015, 2016). Results of the measured solar rotation using CBPs showed more accurate velocity profiles than it was obtained using sunspots and sunspot groups as tracers. Moreover, by using height correction in the measurement of solar rotation previously done by Brajša et al. (2002) using SOHO EIT 284 Å data, Brajša et al. (2004) calculated the average height of the CBPs to be in the range of 8 000–12 000 km above the photosphere, while Sudar et al. (2016) found heights of about 6 500 km using SDO AIA 193 Å data. CBP motions on the solar disk were also used to determine the character of the diffusion of the solar magnetic elements (Brajša et al. 2008, 2015; Skokić et al. 2016, 2019), where it was found that CBP motions are consistent with a subdiffusion process.

Radio observations of CBPs using Very Large Array (VLA) at 6 cm (4.8 GHz) in 1977 showed small-scale compact sources in a range of 9"–25" in diameter with a peak brightness temperature of  $6-8 \times 10^4$  K with respect to the background temperature of  $2 \times 10^5$  K (Marsh et al. 1980). At least half of those sources were associated with bipolar magnetic CBP features. More VLA observations at 6 cm revealed that CBP radio emission shows rapid temporal and spatial variations such as the ones observed in X-rays and EUV (Fu et al. 1987). In the following years, 6 cm and 20 cm observations confirmed that the observed CBP emission came from electron-ion free-free thermal bremsstrahlung (Kundu et al. 1988). Based on the comparison of CBPs observed in soft X-rays by Yohkoh/SXT and at 20 cm by VLA done by Nitta et al. (1992), half of the 33 observed radio sources were associated with XBPs, and the rest were just overlaying magnetically unipolar regions. Another radio observation of CBPs was done by Gopalswamy et al. (1999), and later by Oliveira e Silva et al. (2016), using Nobeyama Radioheliograph (NoRH) at 17 GHz in a study of enhanced microwave brightenings inside polar CHs. These authors found that the enhancement of the radio brightness in CHs at chromospheric heights is explained by the presence of bright patches associated with the presence of intense unipolar magnetic fields. Both previous VLA and NoRH observations show that CBPs are not the only radio source, and that makes it harder to identify CBPs using only radio data. We encountered the similar problem in our work which will be discussed in Sect. 4, where strong bright radio sources could not be distinguished from the nearby CBPs.

Construction of Atacama Large Millimeter/submillimeter Array (ALMA) enabled detailed observations of the solar chromosphere needed to better understand this layer of the solar atmosphere and all the features there (Wedemeyer et al. 2016). ALMA provides observations using both single-dish (White et al. 2017) and interferometric (Shimojo et al. 2017) observing modes, with a wavelength coverage ranging from 0.3 mm and 9 mm, which correspond to the maximum intensity contribution heights of 490 km and 1170 km respectively (Wedemeyer et al. 2016). So far, mostly ~1 mm (Band 6) and ~3 mm (Band 3) wavelengths were used in solar observations in both single-dish and interferometric modes, where some of the Band 6 data will be presented in this study. New observations made by ALMA since the late 2015 show great promise in CBP observations at millimeter and submillimeter wavelengths enabling us to study the CBPs at chromospheric heights.

Earlier ALMA CBP observations done by Shimojo et al. (2017b) using Band 3 channel report first ALMA observation of a solar plasmoid ejection from a CBP that was observed simultaneously in ALMA Band 3, AIA EUV and soft X-rays Hinode/XRT data. They found that the plasmoid consists either of

approximately isothermal  $\sim 10^5$  K plasma that is optically thin at 100 GHz, or else a  $\sim 10^4$  K core with a hot envelope. Another Band 3 observations done by [Rodger et al. \(2019\)](#) using four constituent subbands within Band 3 analyzed logarithmic millimeter spectrum of the plasmoid ejection event near the simultaneous CBP in the active region NOAA12470. These authors concluded that stationary and moving enhancements both lie near the transition between optically thin and thick plasma at 100 GHz. From the estimated optical thicknesses of the two enhancements, isothermal plasmas would be expected to have electron temperatures of  $\sim 7\ 370$ – $15\ 300$  K for the stationary enhancement and  $\sim 7\ 440$ – $9\ 560$  K for the moving enhancement.

Using ALMA Band 6 data, [Brajša et al. \(2018\)](#) reported the first analysis of solar structures in 1.21 mm full-disk solar ALMA images. They compared full-disk solar ALMA image, taken on 18 December 2015, with simultaneous images in optical (H $\alpha$  line), infrared (He I 1083 line) and EUV (AIA 1700Å, 304Å, 211Å, 193Å and 171Å) spectrum as well as with an SDO Helioseismic and Magnetic Imager (HMI) magnetogram. CBPs visible in the observed data showed a very good match with ALMA bright features, where 82% of all CBPs from the EUV image corresponded to the ALMA 1.21 mm bright points. A continuation of this work was done by [Brajša et al. \(2021\)](#) with an emphasis on CBPs in ALMA Band 6 data. In the quiet Sun, four CBPs were identified, with other small-scale ALMA bright features most likely being associated with magnetic network elements and plages. It was also found that enhanced emission seen in ALMA data is almost always associated with strong line-of-sight magnetic field. In the active region, using ALMA Band 3 interferometric data, 14 small-scale ALMA bright features were randomly selected, and by comparing with other wavelength images, they found five CBP, two plage, and five fibril candidates, with only two remaining uncertain features.

In the present paper, which is a continuation of the work done by [Brajša et al. \(2021\)](#), we present an analysis of intensity and sizes of CBPs within the boundaries of five different CHs and of CBPs outside them in the quiet Sun region. We first describe data and methods used for CH extraction and CBP identification, measurement and statistical analysis (Sect. 2). Next, we present the results of CH extraction and statistical analysis of the measured CBP properties (Sect. 3), then discuss and compare the important results (Sect. 4) and finally finish with plans for future work (Sect. 5).

## 2. Data and methodology

### 2.1. ALMA single-dish data

From several hundred full-disk solar images taken by ALMA between 23 March 2017 and 13 April 2019, a total of five images were chosen that contain different CHs near the central region of the solar disk. The five chosen full-disk solar maps for 16 April 2017, 22 April 2017, 17 April 2018, 3 May 2018 and 25 December 2018 were obtained by scanning the solar disk with a 12 m single-dish total power ALMA antenna at Band 6 frequencies 230 GHz ( $\lambda = 1.3$  mm), 248 GHz ( $\lambda = 1.21$  mm), 232 GHz ( $\lambda = 1.29$  mm), 248 GHz ( $\lambda = 1.21$  mm) and 230 GHz ( $\lambda = 1.3$  mm) respectively in a double circle pattern ([Philips et al. 2015](#), [White et al. 2017](#)). We restricted ourselves to only Band 6 because of a better resolution in comparison to other currently available bands used for solar observations with the total power antenna. Single-dish beam sizes for the obtained images are 28.3", 26.7", 28.2", 26.7" and 28.4" respectively with a pixel scale of 3".

Before we could analyze the selected ALMA images, they had to be corrected for the limb brightening effect. For this purpose we used a second-order polynomial fit for the center-to-limb brightness function following the procedure given in [Sudar et al. \(2019\)](#). The limb brightening correction procedure was done using *limb.py* Python script made by [Sudar et al. \(2019\)](#) for the limb brightening correction of ALMA data.

### 2.2. SDO observations

From the available SDO data, we took AIA EUV 193 Å filtergrams ([Lemen et al. 2012](#)) taken at the corresponding observational times of the chosen ALMA images. The spatial resolution for all selected EUV images was 0.6" per pixel. Since the limb brightening effect in the EUV data is very low at distances smaller than 0.7 solar radii from the solar disk centre ([Verbeek et al. 2014](#)), there is no need for the limb brightening correction to be made for the purpose of the CBP measurements if we only search for CBPs in the central regions of the solar disk as it is done in the present paper. The next set of SDO data was HMI data taken at the same times with the spatial resolution of 0.5" per pixel ([Scherrer et al. 2012](#)). HMI data shows magnetograms of the line-of-sight (LOS) magnetic field with a time cadence of 45 s for the whole solar disk. For the purpose of our analysis, the values of the HMI magnetogram intensities were saturated at the values of  $\pm 120$  G to better see the magnetic flux sources in the solar photosphere.

### 2.3. Coronal hole extraction

To extract the boundaries of CHs as well as their intensity and area, but also magnetic properties inside them, we used Collection of Analysis Tools for Coronal Holes (CATCH) developed by [Heinemann et al. \(2019\)](#) as a user-friendly SolarSoftWare Interactive Data Language (SSWIDL) Graphical User Interface (GUI). CATCH uses a threshold based extraction method that incorporates the intensity gradient along the CH boundary. It uses two free parameters that we can manipulate, which are intensity threshold that is based on the median intensity of the solar disk and radius of the morphological operator that smoothes the CH boundary. During image upload, we use the annulus limb brightening effect correction based on [Verbeek et al. \(2014\)](#), which is available in CATCH, and to enhance the processing speed, we down-scaled EUV filtergrams from a pixel scale of  $4096 \times 4096$  to  $2048 \times 2048$ . The best CH boundary was extracted using the evaluation given in [Heinemann et al. \(2019\)](#).

### 2.4. CBP identification

We based our CBP identification on SDO data which includes AIA EUV 193 Å filtergrams and HMI magnetograms. On EUV maps (e.g. Fig. 1) CBPs can be recognized as small-scale bright loop-like structures of plasma that link two photospheric magnetic flux concentrations of opposite polarity visible in magnetogram data. For visualisation of the SDO images we used SunPy<sup>1</sup> software package in Python. Our goal was to search for bright loops of plasma connecting different magnetic flux polarities, which gave us a strong confirmation that the observed feature is a CBP, but this was not always easy. Because CBPs have different shapes and sizes, as well as different intensities, there is a chance that we just might catch a CBP at the moment of its emergence or disappearance when it is hard to recognize

<sup>1</sup> <https://sunpy.org/>

*indication*

related to eq(1) : (not looked at reference, sorry)

- I had expected to see the standard errors being added in quadrature

- I don't see why this procedure is robust (t-test)

bootstrap: in comparison to the first procedure<sup>v</sup>  
I would only expect a significant difference if the distributions of the physical properties are significantly non-normal. Is this the case?

I missed to see the <sup>"raw"</sup> distributions of measured quantities in the various regions. Are too few measurements available to create meaningful histograms?

it. In order to determine with great confidence that the observed feature is truly a CBP, we used the help of JHelioviewer software (Müller et al. 2017). With JHelioviewer we were able to visualise the evolution of the feature of interest through time a couple of hours before and after the time of the observed image. By analysing the change of shape and intensity of the observed feature we were able to confirm with great confidence if the observed feature was a CBP or not.

After the CBP identification was carried out for SDO data, we looked at the ALMA images to try to identify the same CBPs there. CBPs visible in the obtained full-disk ALMA images can be identified as bright ellipsoidal features mainly because of a poor spatial resolution of the available images. The CBP identification was first carried out within the boundaries of the CH of interest for both ALMA and SDO data, and based on the number of CBPs found inside CH, a much larger sample of CBPs was selected in the quiet Sun region outside the CH boundaries far from the limb of the solar disk.

### 2.5. Obtaining CBP physical properties

In this work, we have chosen to study (mean) intensity and morphology (size/diameter and area) of CBPs. To determine the edges of a CBP with better precision, we eliminated the surrounding background plasma by setting the intensity threshold based on the median intensity of a small area centred around the selected CBP of interest. Radius of this small area around the CBP was chosen to have values between 30" and 45" depending on the CBP size (larger CBP required the larger radius) and a possible appearance of a strong bright source nearby (if far from the CBP, the smaller radius is taken, if close to the CBP, then the larger radius is taken). The same procedure was done for both ALMA Band 6 and SDO EUV images. Once the boundaries of the selected CBPs were identified, the mean intensity of all CBP pixels included is measured. The CBP area is determined by counting pixels included within the determined edges, and the size (diameter) of a CBP is taken to be the largest distance between two pixels of a CBP.

### 2.6. Statistical difference of the measured physical properties

To see if there is a statistically significant difference in the measured properties between CBPs within and outside CHs, we use two different methods. The first method is a robust method that uses the expression (e.g. Brajša et al. 1999):

$$\Delta\omega = \omega_1 - \omega_2 > N(M(\omega_1) + M(\omega_2)) \quad \text{see above} \quad (1)$$

where  $\omega_{1,2}$  represent mean values of the observed property for two different data samples,  $M(\omega_{1,2})$  are the corresponding standard errors and  $N = 1, 2, 3$ , etc. A difference of the measured means  $\omega_1$  and  $\omega_2$  is statistically significant on the  $N\sigma$  level if the above criterion is fulfilled for the largest natural number  $N$  possible.

The second method is more precise and uses the unequal variances  $t$ -test (Press et al. 1992). As with the previous method, we try to determine if the means of two data sets are significantly different from each other and by how much. In  $t$ -test statistics, this is characterized by two quantities, a  $t$ -value, corresponding to a distance between the two means in terms of standard deviations, and a  $p$ -value, corresponding to a probability for the obtained result to be coincidental. We should note here that, based on our CBP sample ordering, the negative (positive)  $t$ -value means that the mean value of the measured physical property for the CBPs outside (within) the CH boundaries is higher.

For the purpose of our work, if  $p$ -value  $< 0.05$ , then our two data sets have statistically significant difference between their mean values. Both  $t$ -value and  $p$ -value are obtained using the function `ttest_ind`<sup>2</sup> with an unequal variance option under SciPy<sup>3</sup> software package in Python.

Both methods were conducted on 200 samples, which were randomly generated from the detected CBPs inside and outside of CHs. With that we obtain sample pair of equal size which we use for comparison between CBPs inside and outside of CHs. This procedure is called a bootstrap technique (Efron and Tibshirani 1993), and it was used for all the measured physical properties of the selected CBPs. On top of that, we also repeated the whole procedure on different individual CBP sample sizes to see how the result changes for different numbers of CBPs included in the calculation.

## 3. Results

### 3.1. CH extraction

Five chosen CHs outlined with a boundary obtained with CATCH are shown in Fig. 1 and 2. In both figures, the analyzed CBPs are marked with small circles. Additionally, if a CBP was excluded from a CH by CATCH, but it was still inside the most outer CH boundary, we considered it to be inside the CH.

From CATCH we obtained area, mean EUV intensity, signed mean magnetic field strength, magnetic field skewness (measure of the distinctness of a dominant polarity), signed magnetic flux and magnetic flux balance (ratio of signed to unsigned magnetic flux) within the obtained boundaries of the chosen CHs. The obtained properties for all five CHs, including a number of detected CBPs inside and a number of additionally selected CBPs outside of CHs, are given in Table 1.

From Table 1 we see very similar obtained intensity thresholds for all five CHs, with the minimum of 27 DN being for CH3 and maximum of 33 DN being for CH5. The mean value of the intensity threshold is  $31 \pm 1$  DN. Moreover, all of the chosen CHs have very similar mean EUV intensities, with the minimum being 17.83 DN for CH2 and maximum being 20.48 DN for CH4. The mean value of the mean intensities for all five CHs combined is  $19.27 \pm 0.52$  DN.

Based on the obtained CH area, the smallest of the five CHs is CH1 with 7 confirmed CBPs inside and the largest one is CH4 with 32 confirmed CBPs inside. By comparing the CH area and the number of CBPs inside of CHs, we see that larger CHs in general have higher number of CBPs within their boundaries. The only exception is CH3 which is the second largest CH, but has the second smallest number of CBPs found inside out of all the five CHs. If we do a linear fit between the number density of CBPs in CHs ( $N_{in}/A_{CH}$ ) and the CH area ( $A_{CH}$ ) by ignoring CH3, we get  $N_{in}/A_{CH} \sim 0.1122 \times A_{CH}$  with a Spearman's linear correlation coefficient  $r_S = 0.79$ . This result shows a modest tendency of the number density of CBPs in CHs to increase with CH area. When adding CH3 into consideration, the Spearman's correlation coefficient immediately drops to  $r_S = 0.21$ , showing very weak correlation between the number density of CBPs and CH area. By analyzing the corresponding errors of a CH area, we see that four out of five CHs have stable boundaries with CH2 having the highest stability if we consider the relative error for CH area. We find low stability boundaries only for CH3, with a

<sup>2</sup> [https://docs.scipy.org/doc/scipy/reference/generated/scipy.stats.ttest\\_ind.html](https://docs.scipy.org/doc/scipy/reference/generated/scipy.stats.ttest_ind.html)

<sup>3</sup> <https://scipy.org/>

I do not find it easy to recognize the intensity pattern below the yellow circles. Can we make

*the circle, e.g., semi-transparent?*

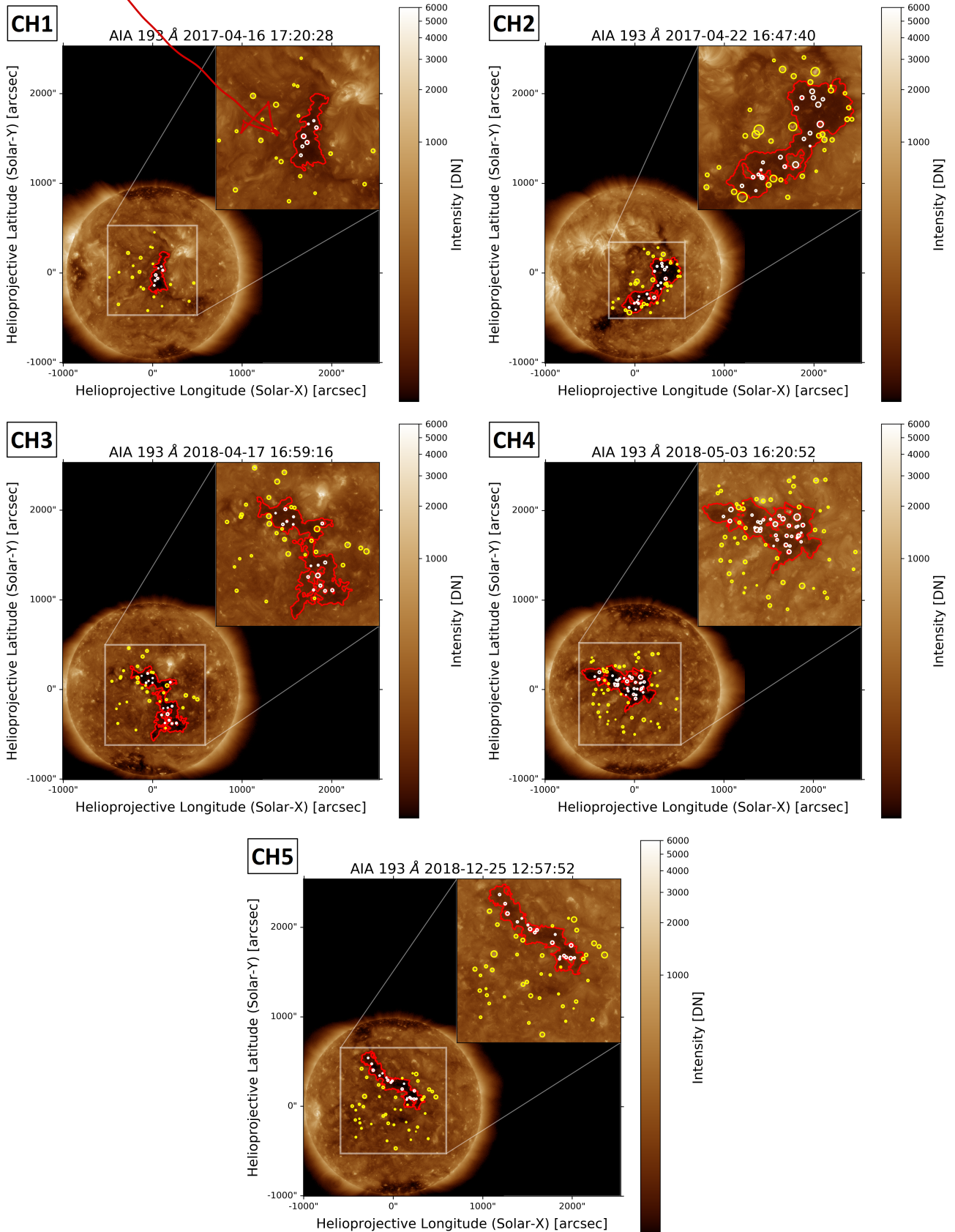


**Fig. 1.** SDO 193 Å EUV full-disk images of the solar corona with five chosen CHs (CH1, CH2, CH3, CH4 and CH5 respectively) outlined with a red boundary obtained with CATCH using the same SDO 193 Å EUV images, while the selected CBPs are marked with circles (white - within CH, yellow - outside CH). Inset images in the top right corner of the full-disk images show a close up look of the central region containing the corresponding CH with all of the selected CBPs. Intensity is clipped between 20 and 6 000 DN.

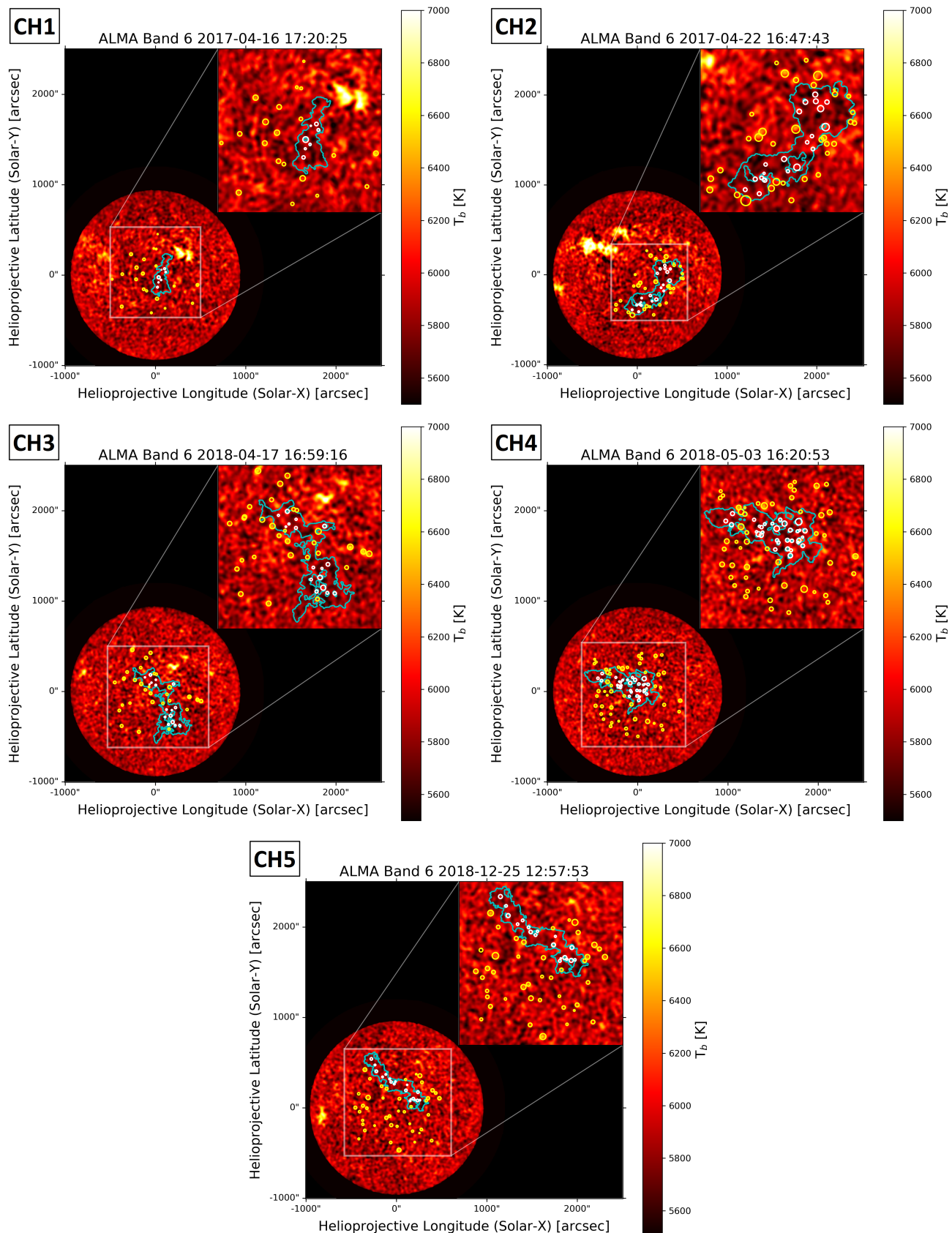


**Fig. 2.** ALMA Band 6 full-disk images of the solar chromosphere with the outlined CHs (red boundary), marked positions of the selected CBPs and with inset images of a close up look of the corresponding CHs and all of the selected CBPs as in Fig. 1. Brightness temperature  $T_b$  is clipped between 5 500 and 7 000 K.

**Table 1.** Properties of the five chosen CHs denoted as CH1, CH2, CH3, CH4 and CH5.

	CH1	CH2	CH3	CH4	CH5
Date of observation [y-m-d]	2017-04-16	2017-04-22	2018-04-17	2018-05-03	2018-12-25
Time of observation [h:m:s]	17:20:28	16:47:40	16:59:16	16:20:52	12:57:52
Intensity threshold [DN]	32	31	27	33	32
Area [ $10^{10}$ km <sup>2</sup> ]	$2.74 \pm 0.23$	$7.65 \pm 0.49$	$8.16 \pm 1.24$	$9.24 \pm 0.65$	$5.93 \pm 0.59$
Mean Intensity [DN]	$20.13 \pm 0.90$	$17.83 \pm 0.75$	$18.29 \pm 1.13$	$19.60 \pm 0.87$	$20.48 \pm 0.99$
Signed mean magnetic field [G]	$2.46 \pm 0.03$	$-1.90 \pm 0.04$	$-1.12 \pm 0.14$	$-2.01 \pm 0.01$	$1.31 \pm 0.07$
Magnetic field skewness	$8.76 \pm 0.30$	$-7.29 \pm 0.22$	$-4.65 \pm 0.34$	$-7.55 \pm 0.08$	$5.99 \pm 0.18$
Signed magnetic flux [ $10^{20}$ Mx]	$5.93 \pm 0.39$	$-13.34 \pm 0.26$	$-7.67 \pm 0.22$	$-18.40 \pm 1.20$	$6.87 \pm 0.35$
Magnetic flux balance [%]	$29.00 \pm 0.42$	$20.80 \pm 0.74$	$13.28 \pm 1.89$	$21.79 \pm 0.10$	$13.92 \pm 0.76$
No. of confirmed CBPs inside of CH	7	21	16	32	18
No. density of CBPs inside of CH [ $10^{-10}$ km <sup>-2</sup> ]	$2.55 \pm 0.21$	$2.75 \pm 0.18$	$1.96 \pm 0.30$	$3.46 \pm 0.24$	$3.04 \pm 0.30$
No. of selected CBPs outside of CH	20	34	30	50	42

relative area error over 15%. This large uncertainty for CH3 is possibly due to its peculiar shape, with a southern patchy structure, that could have also affected the number of CBPs detected inside of it.

Analysis of the magnetic field properties underlying the CHs (Table 1) yielded two CHs (CH1 and CH5) with positive polarity and three CHs (CH2, CH3 and CH4) with negative polarity. We see that the absolute value of the signed magnetic field of the CHs varies only between 1.12 G for CH3 and 2.46 G for CH1 with the mean being  $1.76 \pm 0.24$  G. Absolute value of the skewness of the magnetic field distribution varies between 4.65 for CH3 and 8.76 for CH1, with the total mean value of  $6.85 \pm 0.70$ , showing the asymmetry in the magnetic field distribution of the five CHs caused by the abundance of open magnetic field lines.

The largest difference in magnetic property between these five coronal holes is found in their magnetic field flux. Because the magnetic field strength does not vary much between CHs, it means that the magnetic flux must go with the CH area. The minimum absolute value of  $5.93 \times 10^{20}$  Mx for the signed magnetic field flux is found for CH1, while the maximum of  $18.4 \times 10^{20}$  Mx is found for CH4. Mean value of the absolute signed magnetic field fluxes for all CHs combined is  $10.44 \pm 2.37 \times 10^{20}$  Mx. For the magnetic flux balance, which is a measure of the percentage of open flux, the minimum magnetic flux balance is found for CH3 with a value of only 13.28% and the maximum magnetic flux balance is found for CH1 with a value of 29%. The total mean magnetic flux balance for the five chosen CHs together was found to be  $16.16 \pm 2.89\%$ .

Going forward in the results, we will mostly focus our discussion on the results obtained for CH2 as a good example for the measured CBP properties out of the five CHs, but we will still compare the results between all five CHs. Results of the statistical analysis for the measured CBP properties for CH1, CH3, CH4 and CH5 can be found in Appendix A, B, C and D.

### 3.2. Mean CBP intensity

#### 3.2.1. ALMA data

Based on all of the selected CBPs, the maximum values of the mean intensities for the CBPs within and outside all five CHs in the ALMA Band 6 images are presented in Table 2.

First column of Table 2 shows that CBPs outside the chosen CHs can reach higher values of the mean brightness temperature than the CBPs inside CHs. In all five cases, the average mean brightness temperature (second column of Table 2) for CBPs

**Table 2.** Maximum ( $\bar{I}_{max}$ ) and mean ( $\langle \bar{I} \rangle$ ) values of the mean measured ALMA Band 6 intensities (brightness temperature) of the CBPs within and outside the chosen five CHs.

	$\bar{I}_{max}$ [K]	$\langle \bar{I} \rangle$ [K]
	within CH / outside CH	within CH / outside CH
CH1	6051 / 6433	$5925 \pm 27 / 6138 \pm 30$
CH2	6209 / 6348	$5997 \pm 19 / 6125 \pm 22$
CH3	6201 / 6485	$5963 \pm 25 / 6173 \pm 26$
CH4	6284 / 6431	$6058 \pm 18 / 6112 \pm 17$
CH5	6255 / 6379	$6036 \pm 24 / 6201 \pm 27$

outside the CHs is higher than for those outside, and it reaches values above 6 100 K. On the other hand, for the CBPs inside the CHs the average brightness temperature is below the previous value and in the first three cases even below 6 000 K.

Top left panel of Fig. 3 shows very clearly the separation between CBPs inside and outside CH2, with the ones inside having a lower mean brightness temperature and a smaller mean brightness temperature dispersion around a general mean value (Table 2). By increasing the sample size for bootstrapping, we find a more pronounced separation. Moreover, larger overlaps of the mean brightness temperatures were found for two coronal holes, CH4 and CH5, when having smaller sample sizes.

The histogram in the top right panel of Fig. 3, which was obtained using the expression 1, shows that most of the CBP sample pairs have their brightness temperatures differing between  $2\sigma$  and  $3\sigma$ . Even larger difference is seen in the bottom row of Fig. 3, where in the left panel we see a large number of sample pairs having the mean brightness temperature difference between  $3\sigma$  and  $3.5\sigma$ , with a tendency towards  $3\sigma$ . The  $p$ -values in the right panel show that almost all of the sample pairs have a  $p$ -value under 0.05, clearly showing a statistically significant mean brightness temperature difference between CBPs inside and outside the CH2. Similar results were also found for the remainder of the CHs as well (Fig. A.1, B.1, C.1 and D.1), with a higher or smaller difference visible between CBP inside and outside a CH depending on the CH of interest.

#### 3.2.2. SDO data

Moving onto SDO EUV data, Table 3 presents the results for the maximum value of the mean CBP brightness temperatures obtained for all of the selected CBPs.

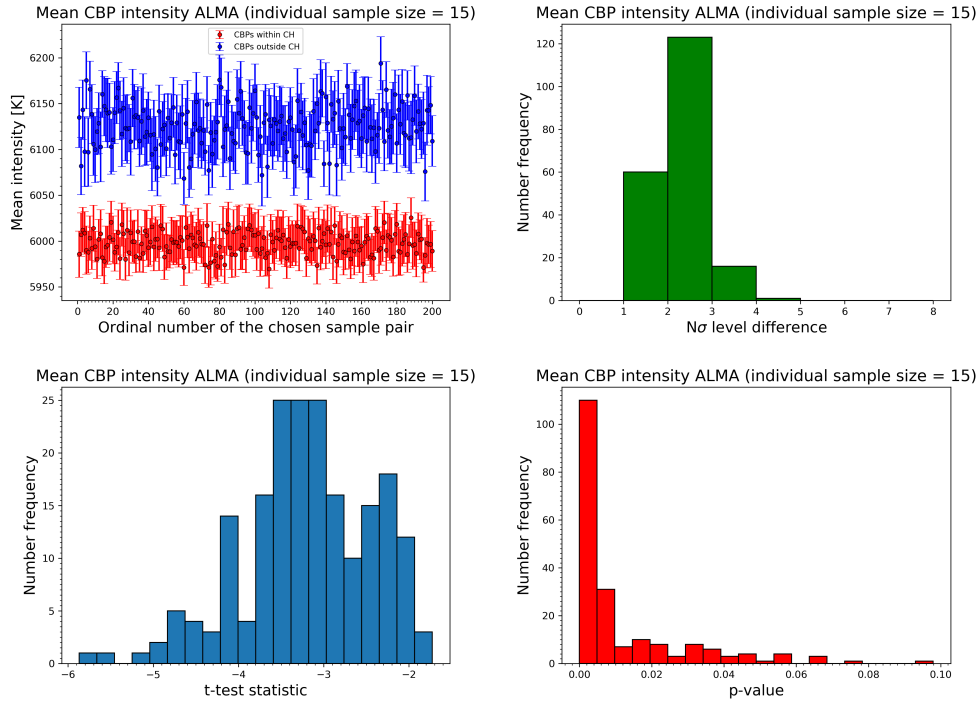


**Fig. 3.** Top row: Left panel shows the mean values of the mean CBP intensities (brightness temperature) in the ALMA Band 6 image with corresponding standard errors of 200 randomly chosen equal size CBP sample pairs, with one sample containing CBPs within (red) and the other outside (blue) the coronal hole, while the right panel shows histogram of the largest  $N$  for which the relation (1) holds true. Bottom row: Left panel shows histogram of the  $t$ -test statistic values ( $t$ -values) and the right panel shows the histogram of the  $p$ -values obtained for the mean values of CBP mean intensities in the ALMA Band 6 image. Individual CBP sample contains 15 randomly chosen CBPs out of the many selected CBPs either within or outside the CH of interest.

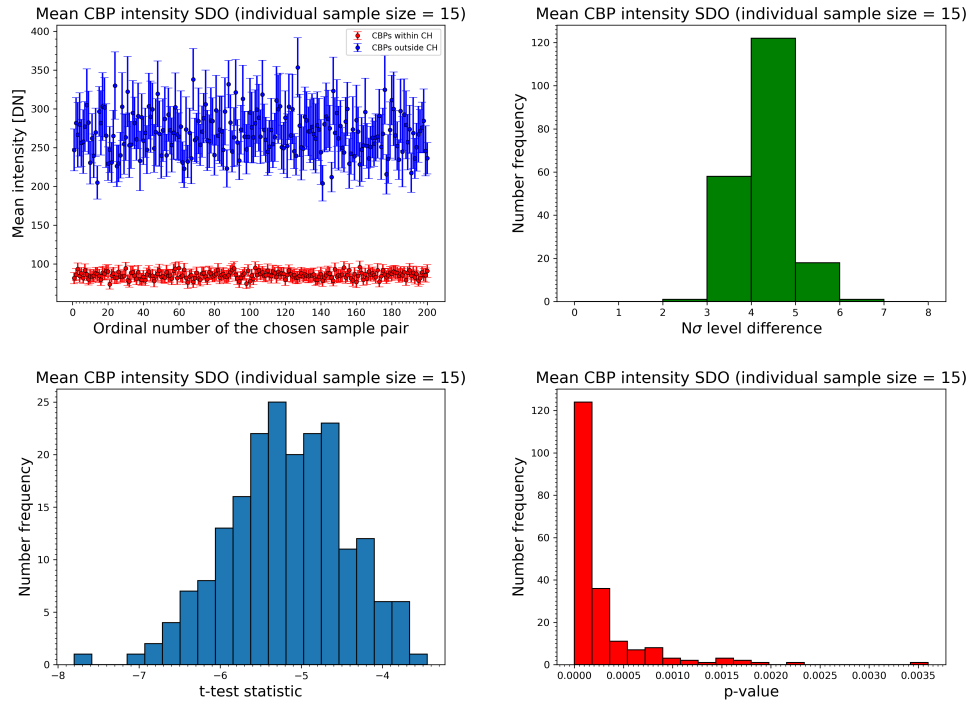


**Fig. 4.** Same as Fig. 3, but for SDO EUV data.

In Table 3 we see similar behaviour between CBPs inside and outside the CH2 as it was the case in Table 2 for ALMA data. The maximum mean EUV intensity (first column of Table

3) for the CBPs within the CH2 is lower in value than we found for the CBPs in the quiet Sun outside the CH2. We see a very high measured EUV intensity for a single CBP outside the CH3

**Table 3.** Same as Table 2, but for SDO EUV data.

	$\bar{I}_{max}$ [DN]	$\langle \bar{I} \rangle$ [DN]
	within CH / outside CH	within CH / outside CH
CH1	109 / 610	$76 \pm 7 / 361 \pm 34$
CH2	142 / 725	$85 \pm 7 / 269 \pm 24$
CH3	175 / 1641	$83 \pm 9 / 347 \pm 52$
CH4	452 / 911	$111 \pm 15 / 289 \pm 21$
CH5	175 / 468	$93 \pm 7 / 210 \pm 12$

with a mean intensity value of 1641 DN. Moreover, we found that all of the average mean intensity values (second column of Table 3) are surpassing 200 DN for CBPs in the quiet Sun outside the CH2 for all five CHs, while for the CBPs inside the CHs the value is under 100 DN, except for the largest coronal hole CH4 for which the average mean EUV intensity value is measured to be 111 DN.

The top left panel of Fig. 4 shows the separation between the CBPs within and outside the CH2 to be more prominent than for the measured mean ALMA intensity seen in Fig. 3. The dispersion of the mean EUV intensity for CBPs inside CH2 is very narrow, around 30 DN in width, while for the CBPs in the quiet Sun outside the CH2 it is much higher. Also, when taking different sample sizes, we found the same effect on the results as it was the case for ALMA data. Just by looking at the top left panel of Fig. 4, we see a very significant difference in the mean EUV intensity between CBPs inside and outside the CH, not only for the current case of CH2, but also for the rest of the selected CHs (Fig. A.4, B.4, C.4 and D.4).

Next, in the top right panel of Fig. 4 we see that the presented histogram shows very similar shape as the one for the mean ALMA intensity (Fig. 3), but with a shift of about  $2\sigma$  to higher values. This time, the largest number of CBP sample pairs have the individual sample mean EUV intensities differing by about  $4\sigma$  to  $5\sigma$ , which suggests this result has a negligible possibility for being coincidental. Bottom row of the Fig. 4 shows even higher difference between the two groups of CBPs, where  $t$ -values show that the largest number of CBP sample pairs are grouped between  $4.5\sigma$  and  $6\sigma$  difference, with a maximum closer to  $5\sigma$ . Moreover, the bottom right panel shows that all 200 randomly chosen sample pairs have a  $p$ -value well under 0.05 threshold. This is a clear indication that the difference in EUV intensity between CBPs inside and outside the CH2 is statistically significant. This was also the case for the rest of the selected CHs (Fig. A.4, B.4, C.4 and D.4), even for small individual sample sizes like the one seen for CH1 (Fig. A.4).

### 3.3. CBP size

#### 3.3.1. ALMA data

Analyzing further, in Table 4 the results of the maximum measured CBP sizes (diameters) and the mean values for all of the selected CBPs in the ALMA Band 6 images for all five selected CHs are presented.

The maximal measured CBP ALMA sizes in Table 4 show a variety of values, where for CH1 and CH4 we have the same measured maximum size for a CBP both within and outside these CHs. For three out of five CHs the maximum size of the CBPs is smaller than for the ones in the quiet Sun outside the CHs, with the largest difference seen for CH5. The maximal measured size for a CBP was found outside the CH2 with a value of 51",

**Table 4.** Maximum ( $d_{max}$ ) and mean ( $\langle d \rangle$ ) values of the measured ALMA Band 6 CBP sizes (diameter) within and outside the chosen five CHs.

	$d_{max}$ [arcsec]	$\langle d \rangle$ [arcsec]
	within CH / outside CH	within CH / outside CH
CH1	35 / 35	$18 \pm 3 / 25 \pm 1$
CH2	38 / 51	$22 \pm 1 / 27 \pm 1$
CH3	35 / 40	$21 \pm 2 / 30 \pm 1$
CH4	46 / 46	$25 \pm 1 / 29 \pm 1$
CH5	29 / 47	$21 \pm 1 / 28 \pm 1$

which is below the agreed maximum size value of 60" for a CBP. Looking at the general mean values of the CBP sizes, we see that CBPs within all five CHs have on average smaller size than the ones outside, with the maximum average size difference seen for CH3, where the average size of CBPs inside the CH3 is 21" and for those outside 30". The minimum average size difference is seen for CH4, where the average size of CBPs inside this CH is 25" and for those outside 29".

Furthermore, the results of the statistical analysis obtained for the measured ALMA Band 6 CBP sizes are presented in Fig. 5. Separation between two different groups of CBPs is visible in the top left panel of Fig. 5, but there are more overlaps of the mean value range than previously seen for CBP intensity. The size dispersion for CBPs within CH2 is around the mean value of 22" and has a smaller width than the CBP group outside CH2 with a mean of about 27". For smaller sample sizes we found more overlaps between the mean values for each CBP sample pair, where the difference between the two means was much smaller. The same behaviour was found for each selected CH (Fig. A.2, B.2, C.2 and D.2), where the separation between the CBP inside and outside the CH was more pronounced for larger CBP sample sizes. The smallest visible separation between these two groups of CBPs was found for CH1 (Fig. A.2), where we have large overlaps between the mean values, but we still see the diversity between CBPs inside and outside the CH1 even for the small CBP sample size.

The histogram in the top right panel of Fig. 5 shows that the difference in CBP size between different groups of CBPs for ALMA data is not very large. We found that the large number of CBP sample pairs have their sizes differing by only  $1\sigma$  to  $2\sigma$ , with a smaller number of them differing more. The bottom row of Fig. 5 however, points to a slightly larger difference. Based on the obtained  $t$ -values, the largest number of 200 sample pairs have the size difference at about  $2\sigma$ , similarly to the result for the previous robust method. Moreover, results for the  $p$ -values in the right panel show the maximum number of sample pairs having  $p$ -value under 0.05, but with a great deal of them over this chosen threshold. The remainder of the CHs also show similar results (Fig. A.2, B.2, C.2 and D.2), with the highest difference between CBPs inside and outside a CH seen for CH3 (Fig. B.2), where the size difference was over  $4\sigma$ .

#### 3.3.2. SDO data

Similar to the previously analysed ALMA data, Table 5 shows the maximum measured CBP size and mean of all the sizes for SDO EUV data.

In comparison to ALMA data, four out of five CHs show that CBPs inside them have smaller maximum size than the ones outside. The only exception is CH4 for which we have a reverse

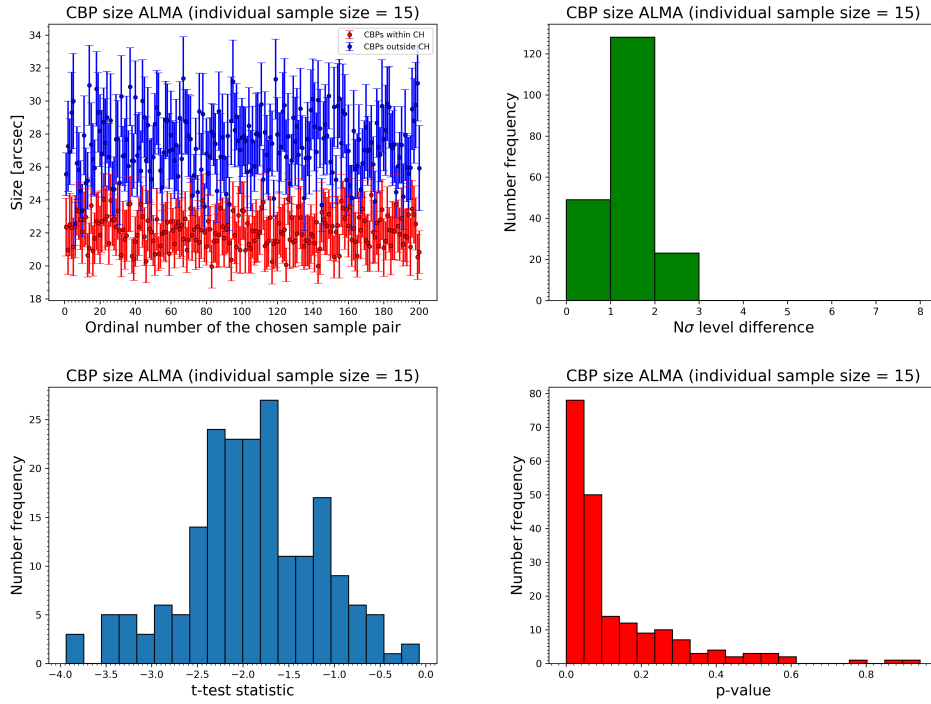


**Fig. 5.** Top row: Left panel shows the mean values of the CBP sizes (diameter) in the ALMA Band 6 image with corresponding standard errors of 200 randomly chosen equal size CBP sample pairs, with one sample containing CBPs within (red) and the other outside (blue) the coronal hole, while the right panel shows histogram of the largest  $N$  for which the relation (1) holds true. Bottom row: Left panel shows histogram of the  $t$ -test statistic values ( $t$ -values) and the right panel shows the histogram of the  $p$ -values obtained for the mean values of CBP sizes in the ALMA Band 6 image. Individual CBP sample contains 15 randomly chosen CBPs out of the many selected CBPs either within or outside the CH of interest.

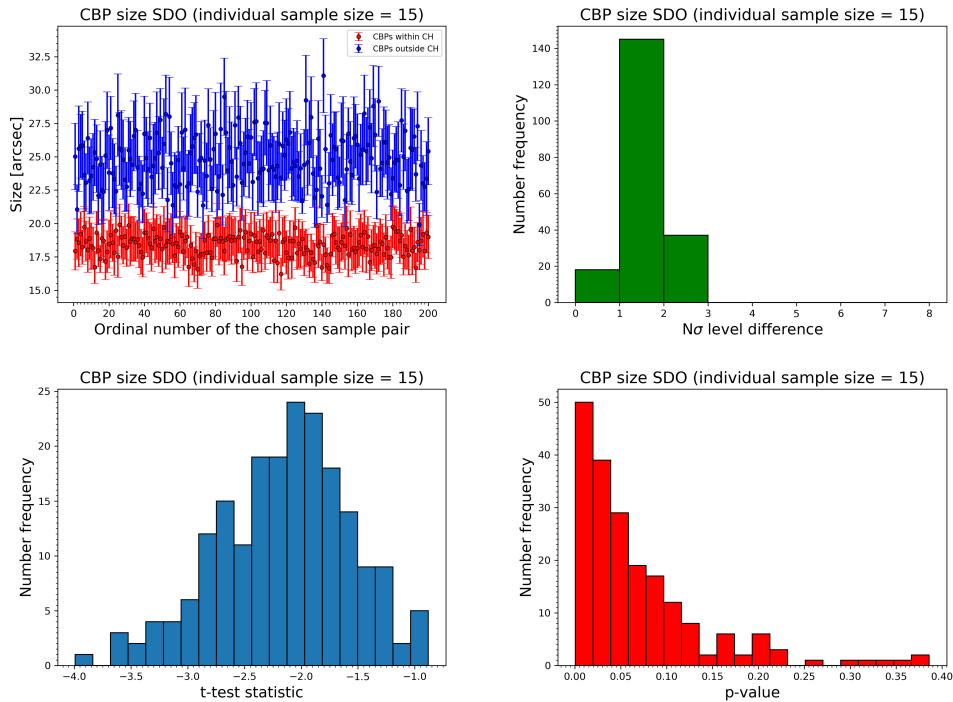


**Fig. 6.** Same as Fig. 5, but for SDO EUV data.

situation where the maximum measured CBP size inside CH4 has a higher value than any of the selected CBPs outside CH4. The maximum measured CBP size for EUV data was found to be 49" for a CBP outside CH2. The mean value of CBP sizes

shows that CBPs inside four of the CHs are on average smaller than those outside, similar to ALMA data. Again, the CH4 is the exception because the obtained average sizes are the same,

**Table 5.** Same as Table 4 but for SDO EUV data.

	$d_{max}$ [arcsec]	$\langle d \rangle$ [arcsec]
	within CH / outside CH	within CH / outside CH
CH1	27 / 31	$18 \pm 2 / 20 \pm 1$
CH2	31 / 49	$18 \pm 1 / 25 \pm 2$
CH3	30 / 37	$16 \pm 1 / 24 \pm 1$
CH4	43 / 37	$20 \pm 1 / 20 \pm 1$
CH5	25 / 43	$18 \pm 1 / 22 \pm 1$

meaning that for this CH there is no clear CBP size difference between the CBPs inside and outside it.

Next, Fig. 6 shows the results of the statistical analysis for the CBP sizes in EUV data, where the separation of the two CBP groups, visible in the top left panel, is now slightly more prominent than it was for ALMA data (Fig. 5). We find lower EUV size dispersion for CBPs inside CH2 in comparison to the ones outside in the quiet Sun region. The CBP size values for CBPs inside CH2 vary around the mean value of 18", while for the ones outside CH2 they vary around 25". A more or less clear separation between the two different CBP groups was found for almost all of the selected CHs, with larger overlaps seen for smaller sample sizes, and of course for CH1, which either way had a very small number of CBPs inside. However, in comparison to all other CHs, for CH4 we found no clear CBP size difference between two different CBP groups even for the largest sample sizes we used (Fig. C.5). This was because for approximately 50% of the cases the CBPs inside the CH4 were found to be on average larger in size than those outside, and for other 50% they were smaller.

The top right panel of the Fig. 6 shows many of chosen CBP sample pairs having the size difference between  $1\sigma$  and  $2\sigma$ , with not so many of them above that range. In the bottom row of the Fig. 6 the obtained  $t$ -values indicate that CBP EUV sizes between two different CBP groups mostly differ by about  $2\sigma$ , as was the case for the previously used robust method which uses Eq. (1). In comparison, the histogram for the obtained  $p$ -values shows the maximum with a larger number of sample pairs having a  $p$ -value under the chosen threshold of 0.05, but with a negligible number of sample pairs having a  $p$ -value above this threshold. This was the case for three out of five CHs, except for CH1 and CH4. For CH1 the EUV size difference was mostly just under  $1\sigma$ , while for CH4 the  $t$ -value histogram distribution had a nice Gaussian shape with the maximum at around  $0\sigma$  for basically every sample size we considered. Moreover, as we took larger and larger sample sizes, so did the shape of the  $p$ -value histogram for CH4 move towards higher values closer to 1, which is the complete opposite situation than we observed for every single other case for all five CHs.

### 3.4. CBP area

#### 3.4.1. ALMA data

Finally, we come to the CBP area measurements, where the maximum measured CBP areas and the means of all the CBP areas for ALMA Band 6 data are presented in Table 6.

Results from Table 6 show a clear difference in the measured ALMA CBP area between CBPs inside and outside the CHs. We see that CBPs inside all five CHs have smaller maximum measured areas, with the highest value found to be over 860 arcsec<sup>2</sup> in the case of CH2. The maximum area for a CBP outside the CH

**Table 6.** Maximum ( $A_{max}$ ) and mean ( $\langle A \rangle$ ) values of the measured ALMA Band 6 CBP areas within and outside the chosen five CHs.

	$A_{max}$ [arcsec <sup>2</sup> ]	$\langle A \rangle$ [arcsec <sup>2</sup> ]
	within CH / outside CH	within CH / outside CH
CH1	584 / 648	$286 \pm 59 / 355 \pm 35$
CH2	863 / 1054	$321 \pm 36 / 458 \pm 40$
CH3	593 / 1043	$281 \pm 37 / 607 \pm 39$
CH4	668 / 1106	$384 \pm 28 / 533 \pm 35$
CH5	533 / 1474	$305 \pm 32 / 531 \pm 44$

was found for CH5 with a value of 1474 arcsec<sup>2</sup>. Mean values of all the measured CBP areas again point to the same situation where CBPs inside the selected CHs have on average smaller areas than the ones outside the CHs, with the smallest difference between CBPs inside and outside a CH of only 69 arcsec<sup>2</sup> found for CH1.

Statistical analysis done for the CBP areas using ALMA Band 6 data is presented in Fig. 7. The top left panel of the Fig. 7 shows a very similar behaviour as it was the case for the CBP size, only this time there is a slightly more pronounced separation between two different CBP groups. The area dispersion for CBPs inside the CH2 is approximately two times smaller than for the ones outside the CH2. Both different CBP group distributions are dispersed around the general mean values mentioned in Table 6, where the mean area value for CBPs in the quiet Sun outside the CH2 is more than 100 arcsec<sup>2</sup> higher than for the ones inside. By changing the individual CBP sample sizes, we found similar behaviour as was the case for the previously measured CBP properties. We also obtained similar results for the rest of the CHs (Fig. A.3, B.3, C.3 and D.3), with a larger overlap between the mean values obtained for CH1 and CH4, but depending on the sample size, with a small or almost no area difference visible between CBPs inside and outside CH4.

Next, the top right panel of Fig. 7 points to a very high number of CBP sample pairs having the area difference between  $1\sigma$  and  $2\sigma$ , with a very small number of them going above  $3\sigma$ . The same result can be seen in the bottom row of Fig. 7, where most of the CBP sample pairs have their areas differing by an amount between  $1.5\sigma$  and  $2\sigma$ . Moreover,  $p$ -value histogram indicates that there is a maximum number of sample pairs with a  $p$ -value under 0.05, but with a large number of them also having  $p$ -values above the chosen threshold. This result clearly indicates a non-significant difference in CBP area between CBPs inside and outside CH2. Analyzing different sample sizes showed that the area difference was more significant for larger samples. Similar results were found for the rest of the CHs, where the area difference for CH1 (Fig. A.3) was even less significant than the one presented here for CH2, while for CH3 (Fig. B.3), CH4 (Fig. C.3) and CH5 (Fig. D.3) we found more significant CBP area difference around  $2\sigma$  to  $3\sigma$  for CH4 and CH5 and even up to  $5\sigma$  for CH3.

#### 3.4.2. SDO data

For SDO EUV data, the maximum CBP area and the means of all the measured CBP EUV areas for are presented in Table 7.

Based on the measured CBP areas in Table 7, we find that CBPs inside four out of five CHs have smaller maximum EUV area than the ones in the quiet Sun outside those CHs, except for the CH4 for which the highest maximum EUV area is found for CBPs inside CH4. Out of all selected CBPs for all five CHs,

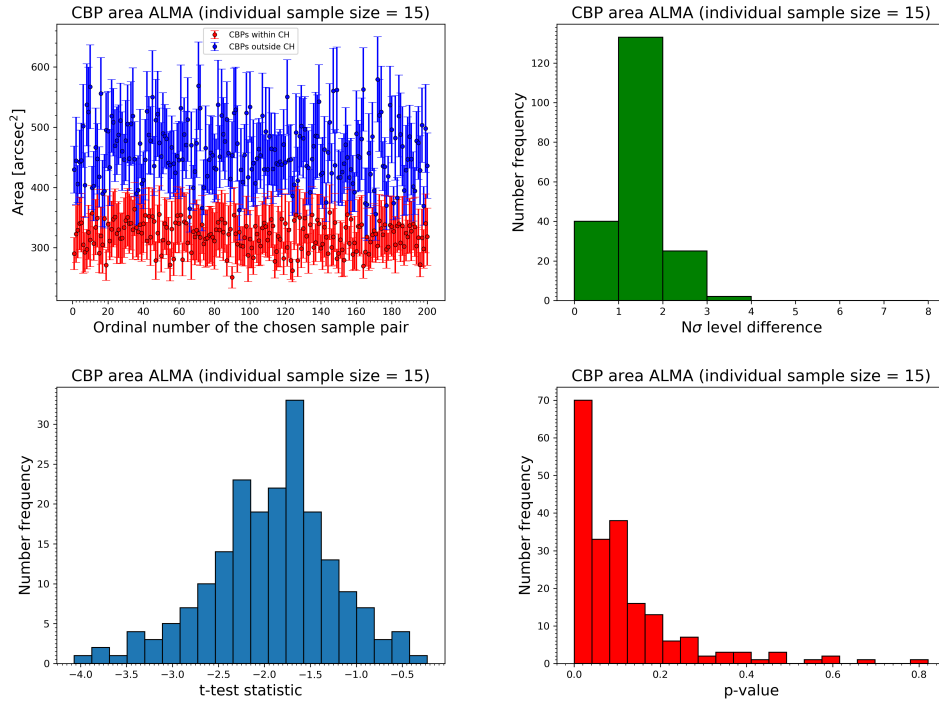


**Fig. 7.** Top row: Left panel shows the mean values of the CBP areas in the ALMA Band 6 image with corresponding standard errors of 200 randomly chosen equal size CBP sample pairs, with one sample containing CBPs within (red) and the other outside (blue) the coronal hole, while the right panel shows histogram of the largest  $N$  for which the relation (1) holds true. Bottom row: Left panel shows histograms of the  $t$ -test statistic values ( $t$ -values) and the right panel shows the histogram of the  $p$ -values obtained for the mean values of CBP areas in the ALMA Band 6 image. Individual CBP sample contains 15 randomly chosen CBPs out of the many selected CBPs either within or outside the CH of interest.

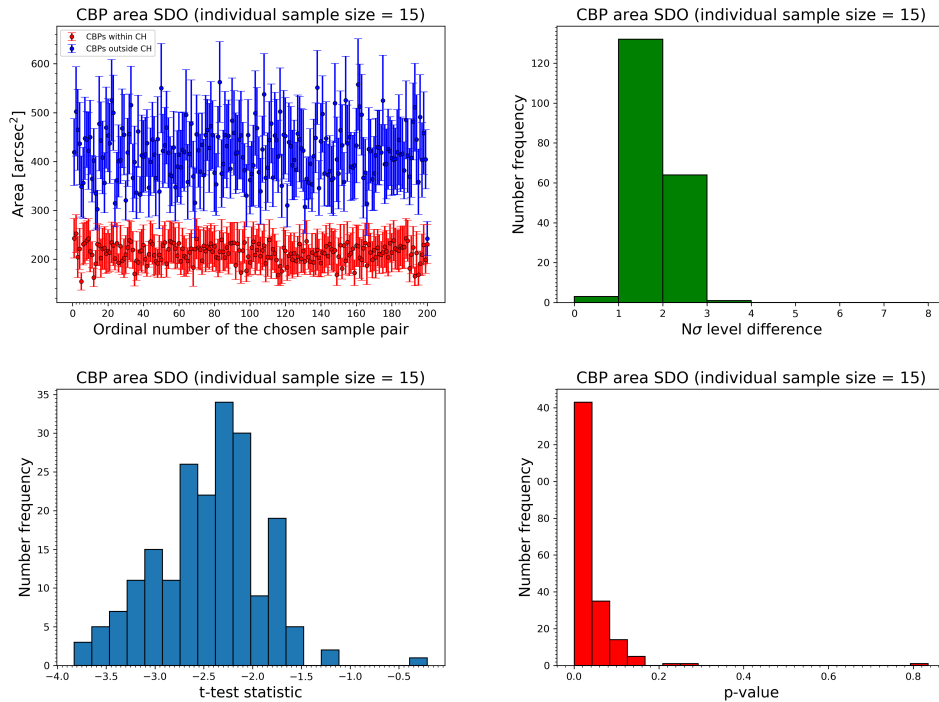


**Fig. 8.** Same as Fig. 7, but for SDO EUV data.

the maximum measured EUV area was found for a CBP outside CH5 with a value of  $1059 \text{ arcsec}^2$ . Similar situation was obtained for the mean value of all the measured EUV areas, where CBPs inside almost all of the CHs have on average smaller EUV, with

the exception of CH4. For CH4 however, the area means have very similar values differing only by  $24 \text{ arcsec}^2$ , meaning that there is no clear difference for the EUV area difference between

**Table 7.** Same as Table 6 but for SDO EUV data.

	$A_{max}$ [arcsec <sup>2</sup> ]	$\langle A \rangle$ [arcsec <sup>2</sup> ]
	within CH / outside CH	within CH / outside CH
CH1	325 / 528	153 ± 36 / 203 ± 31
CH2	675 / 1043	210 ± 31 / 413 ± 49
CH3	377 / 788	138 ± 22 / 345 ± 35
CH4	1002 / 734	226 ± 33 / 250 ± 21
CH5	408 / 1059	175 ± 23 / 285 ± 30

CBPs inside and outside CH4 since the general mean area values basically overlap.

Statistical analysis of the measured EUV CBP areas are presented in Fig. 8. Top left panel of Fig. 8 indicates a much clearer separation between CBPs inside and outside CH2 than it was for the CBP size in Fig. 6. The mean EUV area dispersion is again much smaller for CBPs inside CH2, with a width just above 100 arcsec<sup>2</sup> around the mean value of 210 arcsec<sup>2</sup>, while CBPs in the quiet Sun outside CH2 have three times higher dispersion around the mean of 410 arcsec<sup>2</sup>. Results found for the rest of the CHs (Fig. A.6, B.6, C.6 and D.6) indicate a similar behaviour of the measured EUV CBP area, with more overlaps seen for CH1 (Fig. A.6) and CH4 (Fig. C.6), especially for smaller CBP sample sizes we took. The largest deviation from the results obtained for the rest of the CHs was found for CH4 which had no visible separation between two different groups of CBPs even for some of the large sample sizes, which is connected with the very similar mean area values seen in Table 7. Only for the largest sample sizes taken do we start to see a small separation in CBP EUV area between CBPs inside and outside the CH4.

In the top right panel of Fig. 8 for CH2 we see that the highest number of the CBP sample pairs have their EUV areas differing between  $1\sigma$  and  $2\sigma$ , but there is also a great deal of them having the area difference even between  $2\sigma$  and  $3\sigma$ . The histogram of the obtained  $t$ -value in the bottom row of Fig. 8 however, indicates that the highest number of the CBP sample pairs have CBP areas differing between  $2\sigma$  and  $3\sigma$ , with a maximum of the distribution between  $2\sigma$  and  $2.5\sigma$ . This statistically significant difference is more visible in the  $p$ -value histogram where almost all of the CBP sample pairs have a  $p$ -value under 0.05. Similar results were found for CH3 (Fig. B.6) and CH5 (Fig. D.6) as well, where the EUV area difference goes even up to  $4\sigma$  for CH3. On the other hand, for CH1 (Fig. A.6) and CH4 (Fig. D.6) the EUV area difference was less than  $1\sigma$ , sometimes even less than  $0.5\sigma$ , and the obtained  $p$ -value distributions were, depending on the sample sizes, more or less equally scattered across all the possible values. For these two CHs specifically, the results indicate that there is extremely small, or even no significant difference in the EUV CBP area between the CBPs inside these CHs and the ones outside in the quiet Sun.

## 4. Discussion

### 4.1. CH extraction

In this paper we report measurements of the intensity and sizes of CBPs within the boundaries of five selected CHs at specific times, as well as outside them in the quiet Sun region, with a goal to find if the physical properties differ depending on the region where CBPs reside.

Using CATCH, boundaries of the chosen CHs were extracted and their physical properties (Table 1) were obtained at the time

of observation for SDO EUV data. We find good agreements with the results obtained by Heinemann et al. (2019) for all the measured properties for all selected CH. Also, considering the time of the CH appearance, we find good agreements with the mean values of the physical properties obtained here for CHs at the time of the solar activity decline and minimum.

Comparing the properties of the chosen CHs (Table 1), we find CH4 to stand out from the five chosen CHs in four different properties. This CH is special because it has visibly the largest area out of the five CHs close to  $10^{11}$  km<sup>2</sup> and it contains very large number of CBPs inside it, well above the number found for the other CHs. Moreover, its signed magnetic flux is also larger than those obtained for the other CHs by a large amount. These differences of the CH4 in comparison to other CHs could play a role in the observed CBP properties that we measured, which will be discussed in the upcoming sections.

### 4.2. Mean CBP intensity

In EUV images CBPs appear as bright small-scale coronal loops (Madjarska 2019), while in the ALMA images those same CBPs correspond to bright point features overlaying the bipolar structures seen in the HMI magnetograms (Brajša et al. 2018, 2021). ALMA Band 6 and SDO EUV images in Fig. 2 and 1 show selected CBPs at the certain times the images were taken, where we see a variety of different CBP intensities.

Fig. 3, 4, A.1, A.4, B.1, B.4, C.1, C.4, D.1 and D.4 show visible separation in the mean intensity between the CBPs within CH boundaries and those outside them in the quiet Sun. What we see is that CBPs inside all CHs appear to be fainter than the CBPs outside the CHs in the quiet Sun region in both ALMA and SDO data. Seeing fainter CBPs at both chromospheric and coronal heights could be the consequence of the plasma heating transfer from the upper to bottom parts of a CBP through thermal conduction (Habbal et al. 1990). Based on the means of the mean CBP intensities inside and outside of CHs in both ALMA and SDO data in Table 2 and 3, we derived the relation between relative ratios of mean ALMA ( $\langle \bar{I}_{SDO,in} \rangle / \langle \bar{I}_{SDO,out} \rangle - 1$ ) and SDO intensities ( $\langle \bar{I}_{ALMA,in} \rangle / \langle \bar{I}_{ALMA,out} \rangle - 1$ ) of a form  $\langle \bar{I}_{SDO,in} \rangle / \langle \bar{I}_{SDO,out} \rangle - 1 \sim 5.727 \times \langle \bar{I}_{ALMA,in} \rangle / \langle \bar{I}_{ALMA,out} \rangle - 1$  with  $r_S = 0.63$ . The result shows a modest correlation that could point to the plasma heating being transferred between two different parts of a CBP loop structure, but it is not that strong correlation to rule out the possibility of having different heating mechanisms at different atmospheric layers.

The wider dispersion of the mean intensity for CBPs outside the CHs, for both ALMA Band 6 and SDO EUV data, shows a wider range of possible mean CBP intensities than we have for the CBPs inside the CHs. This indicates that possibly some physical conditions inside CHs, e.g. magnetic field, might limit the intensity seen for a CBP inside a CH. Within CHs, open magnetic field regions are concentrated in unipolar flux tubes covering only a small fraction of up to 10% from the entire CH area (Hofmeister et al. 2017, 2019; Heinemann et al. 2018). The expansion of open magnetic structures within CHs is found to be much stronger compared to the quiet Sun region (Tian et al. 2008). This clearly has effects on the surrounding closed field, where dipole regions with CBPs are formed. Model results confirm that low-lying loops are mostly present within CHs and that they are on average flatter compared to the outside quiet Sun regions (Wiegelmann and Solanki 2004; Wiegelmann et al. 2005). The radially outgoing external field in CHs may "contain" CBPs to smaller heights better than the more random

constrain

to make the expressions look nicer, I suggest to use `\langle` and `\rangle` in math-mode. Moreover, the indices should be set in `\mathit` since they are not mathematical variables but additions to the variable names.

The same holds in many other places of the paper.

fields in the quiet Sun (see Figure 3 in [Wiegelmann et al. 2005](#)). Similar result was found in a recent study by [Heinemann et al. \(2021b\)](#) where the CH magnetic field is derived by using bright bipolar structures in the CH in AIA 304 Å filtergrams, which were also visible in AIA 193 Å filtergrams. The authors found that the strength of the CH magnetic field constrains how large and how far up the bright structures can be, indicating that the appearance of CBPs and the CH magnetic field are linked. Alternatively, the magnetic connectivity environment in a CH is more stable, since the external field is always directed the same way. This might help smaller CBPs last longer against the effects of convective erosion against external fields. Such low-lying CBP loops inside CHs might be related to low plasma flows ([Wiegelmann et al. 2005](#)), revealing a lower temperature/density, or in other words lower intensity. In addition, we observe centrally on-disk located features as line-of-sight integrated intensities, and CBPs in the vicinity of low intensity open flux tubes might appear less bright compared to those located outside CHs. Since CBPs seem to appear in layered structures with different temperatures, where hotter loops are overlaying the cooler loops ([Madjarska 2019](#)), within CHs only the small-scale cooler loops might be present. An emission measure analysis of the CBPs using multiple SDO filters may help decide what combination of factors is driving the intensity differences (beyond the scope of this study).

We also report a smaller difference in the measured mean intensity seen for ALMA data in comparison to SDO data, which was independent of the CBP sample size. This was also true for the CBP sizes and areas. Our results showed larger overlap of the mean value ranges between the CH and quiet Sun CBPs in the majority of the cases. Our assumption is that the modest spatial resolution of the ALMA Band 6 single-dish images might be the main cause of such result. Since the beam width of the analyzed ALMA Band 6 images was about 9 times larger than the pixel size itself, the intensity gradient between any two ALMA features was very small, which prevented us from finding the precise CBP boundary, thus resulting in a much greater uncertainty for the measured properties. However, for all five CHs we found that the mean ALMA brightness temperature for both CBPs inside and outside the chosen CHs are above the central quiet Sun region brightness temperature of 5900 K for Band 6 images ([White et al. 2017](#)), where CBPs inside the CHs had the general mean brightness temperature less than 100 K above the quiet Sun value in three out of five cases (Table 2).

Statistical analysis done using the robust and  $t$ -test method resulted in a very high significance in the difference between the two different CBP groups. The difference between the CBPs inside and outside of all five CHs was between  $2\sigma$  and  $6\sigma$ , similar to the maximum intensity. This indicates that the mean CBP intensity for both ALMA and SDO data at any time, and possibly for any CH, is significantly lower for the CBPs inside CH in comparison to the ones outside CH, indicating that physical conditions, e.g. magnetic field, of the areas where CBPs reside might affect the intensity properties of the CBPs that we observe at any wavelength/height, especially inside CHs where those conditions might prevent CBPs from reaching higher temperatures like we previously discussed.

We also must not exclude the possibility of the influence of CH morphology on the observed intensity. Using the means of the mean CBP intensities ( $\langle \bar{I} \rangle$ ) of all CHs in Table 2 and 3, we find a linear relation between the relative ratio of CBP intensities inside and outside of CHs ( $\langle \bar{I}_{in} \rangle / \langle \bar{I}_{out} \rangle - 1$ ) and CH area ( $A_{CH}$ ) from Table 1. The obtained linear relations

have a form  $\langle \bar{I}_{in} \rangle / \langle \bar{I}_{out} \rangle - 1 \sim 3.76 \times 10^{-3} \times A_{CH}$  with  $r_S = 0.55$  for ALMA and  $\langle \bar{I}_{in} \rangle / \langle \bar{I}_{out} \rangle - 1 \sim 0.0224 \times A_{CH}$  with  $r_S = 0.39$  for SDO data. Spearman's correlation coefficient  $r_S$  for ALMA data shows a modest correlation between the two properties, but for SDO data we see a weak correlation. If we exclude CH3, for ALMA data we get  $r_S = 0.96$  and for SDO data  $r_S = 0.63$ , where we now have a stronger correlation, showing that the relative intensity ratio rises with CH area. Better correlation, with CH3 included, was found if we use number density of CBPs inside CHs ( $N_{in}/A_{CH}$ ) instead of CH area, where we obtain  $\langle \bar{I}_{in} \rangle / \langle \bar{I}_{out} \rangle - 1 \sim 0.133 \times N_{in}/A_{CH}$  with  $r_S = 0.84$  for ALMA and  $\langle \bar{I}_{in} \rangle / \langle \bar{I}_{out} \rangle - 1 \sim 0.0238 \times N_{in}/A_{CH}$  with  $r_S = 0.76$  for SDO data. This result shows a strong correlation between the two properties, indicating the increase in the relative intensity ratio with the number density of CBPs within CHs. This approach with the correlation between the average properties does suffer from small number of CHs, but its results encourage us to analyze the correlation between physical properties of CBPs and a larger number of CHs in more detail in a future work.

Furthermore, we report that individual CBP sample size influences the difference seen between the CBPs inside and outside CHs seen not just for the intensity, but for the sizes and areas of the CBPs as well. Taking larger sample sizes closer to the maximal number of CBPs found inside a CH, with the exception of CBP size in the case of CH4, resulted in a more pronounced difference seen between the CBPs inside and outside CHs, where the mean value ranges barely, or did not even overlapped at all. Based on this result, we recommend using larger samples containing the number of CBPs closer to a number of them inside the CH of interest to maximise the observed difference in physical CBP properties between the two different groups of CBPs.

#### 4.3. CBP size

Size of the selected CBPs follows the similar behaviour seen for the CBP intensity. Fig. 5, 6, A.2, B.2, B.5, C.2, D.2 and D.5 show a separation between the CBPs inside and outside the selected CHs, which indicates that the CBPs inside CHs are on average smaller in size than the ones outside CHs. This is true for both ALMA and SDO data in a majority of the cases. The CBP size dispersion around the general mean value shows CBPs outside the CH boundaries having a wider range of sizes, meaning that those CBPs can possibly grow to much bigger sizes than the CBPs inside the CHs. This is possibly because of the effect of the CH open magnetic structure on the surrounding closed field inside the CH discussed in the Sect. 4.2.

Two out of five CHs, CH1 and CH4, were found to have not very significant differences in CBP size between the CBPs inside and outside CH. This was more pronounced for the analyzed SDO data in comparison to ALMA data. Fig. A.2 and A.5 show the results of the statistical analysis of the CBP size for CH1, where we see that the uncertainty of the mean size is very high, with a more pronounced separation between the two different CBP groups visible for ALMA data, even though it had poor spatial resolution. Fig. A.5 for SDO data clearly shows that there is almost no difference in CBP size between the two different CBP groups, where the difference is less than  $1\sigma$ . This result for CH1 is most likely because the CH1 itself had only 7 CBPs inside it (Table 1), and that number limited the maximum CBP sample size we could take for the purposes of the statistical analysis, thus causing such a great uncertainty and not so significant difference in CBP size.

The situation for CH4 is somewhat different. Fig. C.2 for ALMA data shows a clear separation of about  $2\sigma$  between the CBPs inside and outside of CH4. However, Fig. C.5 for SDO data shows no significant difference in CBP size between those CBPs at all. Histograms on the same figure indicate that the EUV size difference is around  $0.1\sigma$ , where  $t$ -value distribution shows a clear Gaussian shape around that value. The difference in comparison to CH1 here is that CH4 had the largest number of CBPs inside surpassing even 30 CBPs. By changing the CBP sample size to higher and higher values,  $p$ -value distribution for CH4 moved toward right to higher values instead toward left to lower values what we would expect to happen and as it was in other cases. There are couple of possible causes of such an insignificant difference seen between CBPs, e.g. the morphology of the CH4, or maybe magnetic field structure and strength. We know from Table 1 that CH4 is different than the other CHs we observed because of its strong signed magnetic flux, which leads to a conclusion that the underlying CH magnetic field might affect the observed CBP size. Aside from the CH1 and CH4, our results show about  $2\sigma$  in most of the cases to even above  $4\sigma$  (Fig. B.2) difference in the CBP size between the CBPs inside and outside the CHs, with the CBPs inside the CHs having significantly smaller size. This again indicates that certain physical properties, e.g. the previously mentioned magnetic field, of the regions where CBPs reside might affect their sizes.

Nevertheless, based on our CBP size results, we found that the CBP size for the ones inside CHs, when considering all five selected CHs, ranges between 8" and 46" for ALMA data and between 8" and 43" for SDO data. For the CBPs outside CHs, the size ranges between 9" and 51" for ALMA data and between 7" and 49" for SDO data. The total CBP size range, when considering both CBPs inside and outside CHs, was between 7" and 49" in SDO data and between 8" and 51" in ALMA data. These size ranges are in a good agreement with the past observations (Madjarska 2019, Mou et al. 2018) that limit the CBP size between 5" and 60", despite the observed wavelength.

The modest spatial resolution of the ALMA Band 6 full-disk solar images does limit the minimum CBP size we can see in those images. Moreover, because of the modest spatial resolution, discussed in Sect. 4.2, the chosen intensity thresholds to extract CBP pixels used in this study could have produced larger measured ALMA CBP sizes than they truly are, so we have to take those size measurements with a grain of salt. The same is true for the measured CBP areas.

Given the spatial resolution of the ALMA full-disk images, two spatially close features might merge into a single larger object unabling us to determine the properties of each feature individually. This was true in couple of our cases when we had strong unipolar magnetic flux concentration near a CBP. This made intensity and size measurements very difficult since we did not know the exact CBP boundary, so we had to look for any intensity gradient change location on the whole feature to take it as a possible boundary between the individual objects. Also, the location of the opposite magnetic flux polarities of a CBP and the location of the unipolar magnetic flux concentration nearby helped in determining the possible CBP boundaries.

#### 4.4. CBP area

Measured CBP areas follow the results seen for the CBP sizes. Fig. 7, 8, A.3, B.3, B.6, C.3, D.3 and D.6 show a clear separation in CBP area between the CBPs inside and outside all five CHs. We find that CBPs inside the boundaries of CHs have on average smaller areas than those outside in the quiet Sun, that have a

wider range of possible areas, which is directly connected with the wider range of CBP sizes.

Again we found that CH1 and CH4 don't have very significant differences in CBP area as it was the case with the CBP sizes as well. For CH1 this is visible for both ALMA (Fig. A.3) and SDO (Fig. A.6) data, and more so for SDO data. We discussed before the problem of small number of CBPs inside CH1 to be the cause of a small size difference and we believe the problem is the same for the CBP area, where the area difference between the two different CBP groups was around  $1\sigma$ .

In the case of CH4, for ALMA data we do have a significant CBP area difference between the CBPs inside and outside the CH4, but not for SDO data. Only for the larger CBP samples (Fig. C.6) do we see the appearance of an extremely small separation in SDO data between the CBPs inside and outside the CH4 of mostly around  $0.5\sigma$ , with a smaller number of CBP pairs going up to  $1\sigma$ . We believe that the previously discussed difference of the CH4 in comparison to other CHs is the possible cause of the observed insignificant difference in CBP area as it was for CBP sizes. There is also a small chance that we just might have stumbled upon a specific time when the area and size differences between the CBPs inside and outside the CH4 were not significant, although this is very unlikely to happen.

Since the majority of the results for five selected CHs point to a difference in CBP area between the CBPs inside and outside CHs in a range between  $1\sigma$  and even up to  $5\sigma$  (Fig. B.3), this clearly shows that there is a significant difference in CBP area between the two CBP groups, with the ones inside the CHs being on average smaller in area as in sizes, again pointing to an influence of the certain mentioned physical properties of the regions where CBPs reside.

Based on 41 CBPs analyzed in the quiet Sun region of size  $780'' \times 780''$  in the SOHO EIT 195Å passband, Zhang et al. (2001) found an average CBP area of about  $196 \text{ arcsec}^2$ . On the other hand, Alipour and Safari (2015) analyzed statistical properties of CBPs in SDO AIA 193Å data using the maximum CBP size threshold of 56" and found that the average CBP area was around  $225 \text{ arcsec}^2$ . If we combine our results of the CBP areas for both the CBPs inside and outside CHs seen in Table 7 for SDO data, the total mean CBP areas are in a very good agreement with the two previously mentioned values, but with a much better agreement with Alipour and Safari (2015) for four out of five CHs. Areas obtained for ALMA data in Table 6 show a much greater value of CBP area for both CBPs inside and outside CHs when comparing to both previously mentioned sizes, and our EUV sizes as well, possibly because of the modest spatial resolution of ALMA images, which was discussed previously in Sect. 4.3.

## 5. Conclusion and prospects

Based on the obtained results of the measured CBP properties (intensity, size and area) and their analysis, we conclude that CBPs inside the CHs on average have lower intensities than the CBPs outside them in the quiet Sun region, but are also smaller in both size and area. We find this to be true for CBPs visible both at chromospheric heights in ALMA Band 6 data and at coronal heights in SDO EUV data used in this study.

We also find that larger CHs tend to have larger numbers of CBPs inside their boundaries. The morphology of the CH itself could affect the number of CBPs inside, as it was most likely the case for the second largest CH (CH3) for which we found the second smallest number of CBPs within its boundaries out

of the five CHs. The possible influence of the CH morphology on the number of CBPs will be investigated in our future work.

Given the effect of the spatial resolution of the ALMA Band 6 images on the carried measurements of the CBP physical properties discussed in Sect. 4, we conclude that, in order to obtain more precise measurements, the interferometric ALMA data should be used instead of single-dish data that we used in our work. Such data will be of great importance for the future study of the evolution of CBPs inside and outside CHs through time at chromospheric heights.

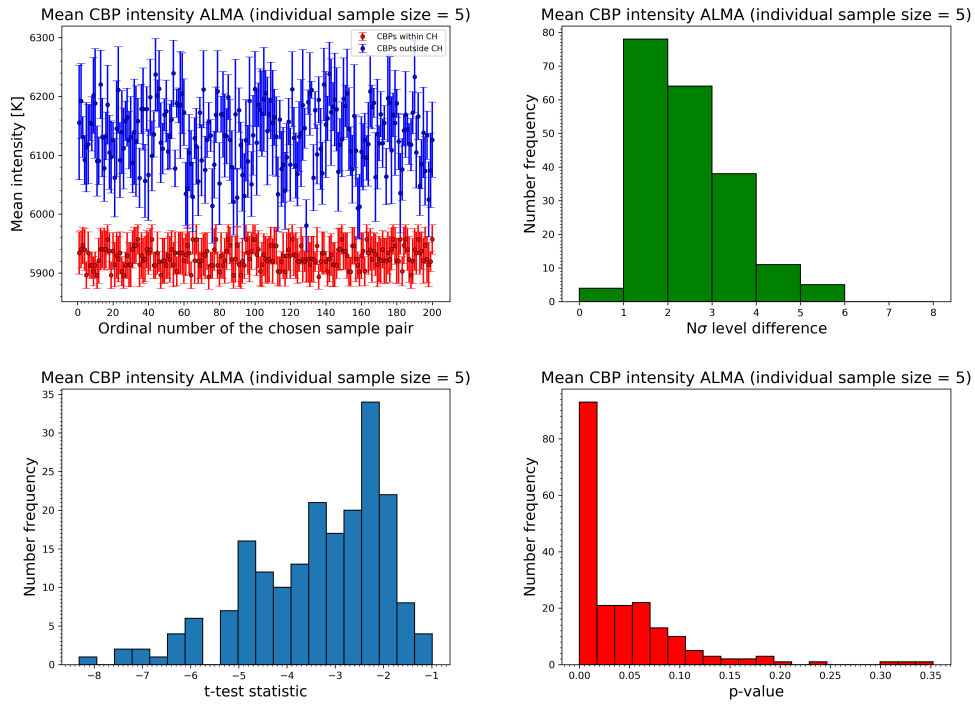
Detailed analysis of the CBP areas and sizes, but also CH properties, for a longer time period, instead of just one specific time as we observed, will be carried out in the future work. Moreover, we plan to follow the evolution of intensity, morphological and magnetic properties of not only CBPs, but CHs as well, where we plan to use interferometric ALMA data mentioned previously, with the available SDO AIA and HMI data at the corresponding times of ALMA observations. Further study will focus on the magnetic field and morphology of CHs in great detail in order to confirm if the CH magnetic and morphological properties influence the observed CBP physical properties, mainly CBP intensity and sizes. If the influence appears to be true, we will investigate how the strength and structure of the magnetic field around the CBPs inside CHs, but also the shape and size of the CHs, affect the observed CBP properties.

*Acknowledgements.* This work has been supported by the Croatian Science Foundation as part of the „Young Researchers’ Career Development Project - Training New Doctorial Students” under the project 7549 “Millimeter and submillimeter observations of the solar chromosphere with ALMA”. It has also received funding from the Horizon 2020 project SOLARNET (824135, 2019–2022). RB and MT acknowledge the support from the Austrian-Croatian Bilateral Scientific Project “Comparison of ALMA observations with MHD-simulations of coronal waves interacting with coronal holes” (2020-2021). In this work ALMA data ADS/JAO.ALMA#2016.1.00050.S, ADS/JAO.ALMA#2016.1.00202.S, ADS/JAO.ALMA#2017.1.00009.S, ADS/JAO.ALMA#2017.1.01138.S and ADS/JAO.ALMA#2018.1.00199.S were used. We also acknowledge the use of the ALMA Solar Ephemeris Generator (Skokić and Brajša 2019). ALMA is a partnership of ESO (representing its member states), NSF (USA) and NINS (Japan), together with NRC (Canada), MOST and ASIAA (Taiwan), and KASI (Republic of Korea), in cooperation with the Republic of Chile. The Joint ALMA Observatory is operated by ESO, AUI/NRAO and NAOJ. We are grateful to the ALMA project for making solar observing with ALMA possible. SDO is the first mission launched for NASA’s Living With a Star (LWS) Program. This research used version 3.1.3 (10.5281/zenodo.3633844) of the Matplotlib open source software package (Hunter 2007), version 1.7.3 (10.5281/zenodo.5725464) of the SciPy open source software package (Virtanen et al. 2020) and version 2.0.5 (10.5281/zenodo.4292495) of the SunPy open source software package (The SunPy Community et al. 2020).

## References

Alipour, N., Safari, H. 2015, *Astrophys. J.* 807:175  
 Bellot Rubio, L., Orozco Suárez, D. 2019, *Living Reviews in Solar Physics*, 16, 1  
 Brajša, R., Skokić, I., Sudar, D., Benz, A. O., Krucker, S., Ludwig, H.-G., Saar, S. H., & Selhorst, C. L. 2021, *A&A*, 651, A6  
 Brajša, R., Sudar, D., Skokić, I., Saar, S. H., Žic, T. 2015, *Cent. Eur. Astrophys. Bull.*, 39, 21  
 Brajša, R., Sudar, D., Benz, A. O., et al. 2018, *A&A*, 613, A17  
 Brajša, R., Ruždjak, R. V., Vršnak, B., Wöhl, H., Pohjolainen, S., Urpo, S. 1999, *Sol. Phys.*, 184: 281–296  
 Brajša, R., Wöhl, H., Vršnak, B., et al. 2002, *A&A*, 392, 329  
 Brajša, R., Wöhl, H., Vršnak, B., et al. 2004, *A&A*, 414, 707  
 Brajša, R., Wöhl, H., Vršnak, B., et al. 2008, *Cent. Eur. Astrophys. Bull.*, 32, 165  
 Cranmer, S. R. 2009, *Living Reviews in Solar Physics*, 6, 3  
 Del Zanna, G., Mason, H. E. 2018, *Living Reviews in Solar Physics*, 15, 5  
 Dere, K. P. 2020, *MNRAS*, 496, 2334-2345  
 Efron, B., Tibshirani, R. J. 1993, *An Introduction to the Bootstrap*, Chapman and Hall, New York

Fu, Q., Kundu, M. R., Schmahl, E. J. 1987, *Sol. Phys.*, 108, 99–111  
 Golub, L., Krieger, A. S., Harvey, J. W., Vaiana, G. S. 1977, *Sol. Phys.*, 53, 111–121  
 Golub, L., Pasachoff, J. M. 2010, *The Solar Corona*, Cambridge University Press, 2nd edition, Cambridge, UK  
 Gopalswamy, N., Shibasaki, K., Thompson, B. J., Gurman, J., DeForest, C. 1999, *Journal of Geophys. Research*, vol. 104, A5, 9767-9779  
 Habbal, S. R., Grace, E. 1991, *Astrophys. J.* 382:667–676  
 Habbal, S. R., Withbroe, G. L. 1981, *Sol. Phys.* 69:77–97  
 Harvey, K. L. 1984, Solar cycle variation of ephemeral active regions. In: Guyenne, T. D., Hunt, J. J. (eds) *The hydromagnetics of the Sun*, ESA SP-220, 235-236  
 Harvey, K. L. 1985, *Aust. J. Phys.* 38:875–883  
 Harvey, K. L., Strong, K. S., Nitta, N., Tsuneta, S. 1994, *Solar Active Region Evolution: Comparing Models with Observations* ed K. S. Balasubramaniam and G. W. Simon (San Francisco, CA: ASP) 377  
 Habbal, S. R., Withbroe, G. L., Dowdy, J. F. Jr. 1990, *Astrophys. J.* 352:333–342  
 Harvey, K. L., Harvey, J. W., Martin, S. F. 1975, *Sol. Phys.*, 40, 87–102  
 Heinemann, S. G., Hofmeister, S. J., Veronig, A. M., Temmer, M. 2018, *Astrophys. J.* 863, 29  
 Heinemann, S. G., Saqri, J., Veronig, A. M., Hofmeister, S. J., Temmer, M. 2021, *Sol. Phys.*, 296, 18  
 Heinemann, S. G., Temmer, M., Heinemann, N., Dissauer, K., Samara, E., Jerčić, V., Hofmeister, S. J., & Veronig, A. M. 2019, *Sol. Phys.*, 294, 144  
 Heinemann, S. G., Temmer, M., Hofmeister, S. J., Stojakovic, A., Gizon, L., Yang, D. 2021, *Sol. Phys.*, 296, 141  
 Hofmeister, S. J., Utz, D., Heinemann, S. G., Veronig, A., Temmer, M. 2019, *A&A*, 629, A22  
 Hofmeister, S. J., Veronig, A., Reiss, M. A., Temmer, M., Vernerstrom, S., Vršnak, B., Heber, B. 2017, *Astrophys. J.* 835, 268  
 Hunter, J. D. 2007, *Computing in Science & Engineering*, 9, 3, 90-95  
 Kundu, M. R., Schmahl, E. J., Fu, Q. -J. 1988, *Astrophys. J.* 325:905-911  
 Lemen, J. R., Title, A. M., Akin, D. J., et al. 2012, *Sol. Phys.*, 275, 17  
 Madjarska, M. S. 2019, *Living Reviews in Solar Physics*, 16, 2  
 Madjarska, M. S., Galsgaard, K., Mackay, D. H., Koleva, K., Dechev, M. 2020, *A&A*, 643, A19  
 Marsh, K. A., Hurford, G. J., Zirin, H. 1980, *Astrophys. J.* 236:1017-1025  
 Mou, C., Huang, Z., Xia, L., et al. 2016, *Astrophys. J.*, 818, 9  
 Mou, C., Madjarska, M. S., Galsgaard, K., Xia, L. 2018, *A&A*, 619, A55  
 Müller, D., Nicula, B., Felix, S., et al. 2017, *A&A*, 606, A10  
 Nitta, N., Bastian, T. S., Aschwanden, M. J., Harvey, K. L., Strong, K. T. 1992, *Publ. Astron. Soc. Japan* 44, L167–L172  
 Oliveira e Silva, A. J., Selhorst, C. L., Simões, P. J. A., Giménez de Castro, C. G. 2016, *A&A*, 592, A91  
 Phillips, N., Hills, R., Bastian, T., et al. 2015, in *Revolution in Astronomy with ALMA: The Third Year*, eds. D. Iono, K. Tatematsu, A. Wootten, L. Testi, et al., ASP Conf. Ser., 499, 347  
 Press, W. H., Teukolsky, S. A., Vetterling, W. T., Flannery, B. P. 1992, *Numerical recipes in C: the art of scientific computing*, 2nd edn. Cambridge University Press, Cambridge  
 Reale, F. 2014, *Living Reviews in Solar Physics*, 11, 4  
 Rodger, A. S., Labrosse, N., Wedemeyer, S., et al. 2019, *Astrophys. J.*, 875, 163  
 Scherrer, P. H., Schou, J., Bush, R. I., et al. 2012, *Sol. Phys.*, 275, 207  
 Shimojo, M., Bastian, T., Hales, A., et al. 2017a, *Sol. Phys.*, 292, 87  
 Shimojo, M., Hudson, H. S., White, S. M., Bastian, T. S., Iwai, K. 2017b, *Astrophys. J.*, 841, L5  
 Skokić, I., Brajša, R. 2019, *Mining-geological-petroleum engineering bulletin*, 34, 2  
 Skokić, I., Brajša, R., Sudar, D., Ruždjak, D., Saar, S. H. 2019, *Astrophys. J.*, 877, 142  
 Skokić, I., Sudar, D., Saar, S. H., Brajša, R., Poljančić-Beljan, I. 2016, *Cent. Eur. Astrophys. Bull.*, 40, 23  
 Sudar, D., Brajša, R., Skokić, I., Benz, A. O. 2019, *Sol. Phys.*, 294, 163  
 Sudar, D., Saar, S. H., Skokić, I., Poljančić Beljan, I., Brajša, R. 2016, *A&A*, 587, A29  
 Sudar, D., Skokić, I., Brajša, R., Saar, S. H. 2015, *A&A*, 575, A63  
 The SunPy Community et al. 2020, *Astrophys. J.*, 890, 68  
 Tian, H., Marsch, E., Tu, C.-Y., Xia, L.-D., He, J.S. 2008, *A&A* 482, 267–272  
 Vaiana, G. S., Krieger, A. S., Van Speybroeck, L. P. and Zennpfennig, T. 1970. *Bull. Am. Phys. Soc.*, 15, 611  
 Verbeeck, C., Delouille, V., Mampaey, B., De Visscher, R. 2014, *A&A*, 561, A29  
 Virtanen, P. et al. 2020, *Nature Methods*, 17, 261-272  
 Wedemeyer, S., Bastian, T., Brajša, R., et al. 2016, *Space Sci. Rev.* 200  
 White, S. M., Iwai, K., Phillips, N. M., et al. 2017, *Sol. Phys.*, 292, 88  
 Wiegmann, T., Solanki, S. K. 2004, *Sol. Phys.*, 225, 227-247  
 Wiegmann, T., Xia, L. D., Marsch, E. 2005, *A&A*, 432, L1  
 Wöhl, H., Brajša, R., Hanslmeier, A., Gissot, S. F. 2010, *A&A*, 520, A29  
 Zhang, J., Kundu, M. R., White, S. M. 2001, *Sol. Phys.* 198:347–365

**Appendix A: Statistical analysis of the physical properties for CBPs within and outside CH1**


**Fig. A.1.** Top row: Left panel shows the mean values of the mean CBP intensities (brightness temperature) in the ALMA Band 6 image with corresponding standard errors of 200 randomly chosen equal size CBP sample pairs, with one sample containing CBPs within (red) and the other outside (blue) the CH1, while the right panel shows histogram of the largest  $N$  for which the relation (1) holds true. Bottom row: Left panel shows histogram of the  $t$ -test statistic values ( $t$ -values) and the right panel shows the histogram of the  $p$ -values obtained for the mean values of CBP mean intensities in the ALMA Band 6 image. Individual CBP sample contains 15 randomly chosen CBPs out of the many selected CBPs either within or outside the CH1.

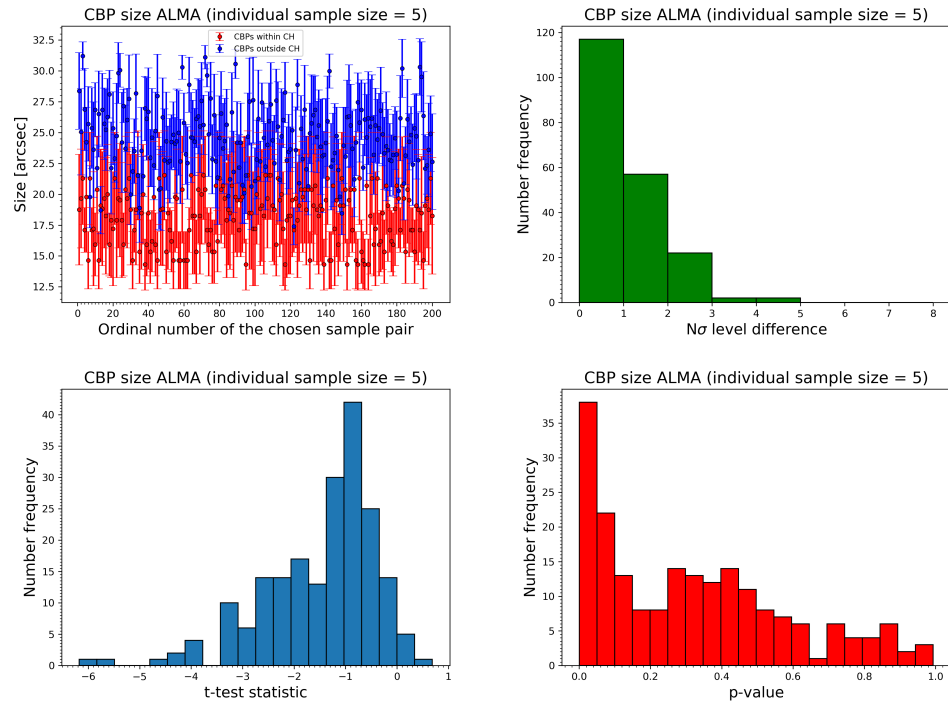


**Fig. A.2.** Same as Fig. A.1, but for the CBP size.

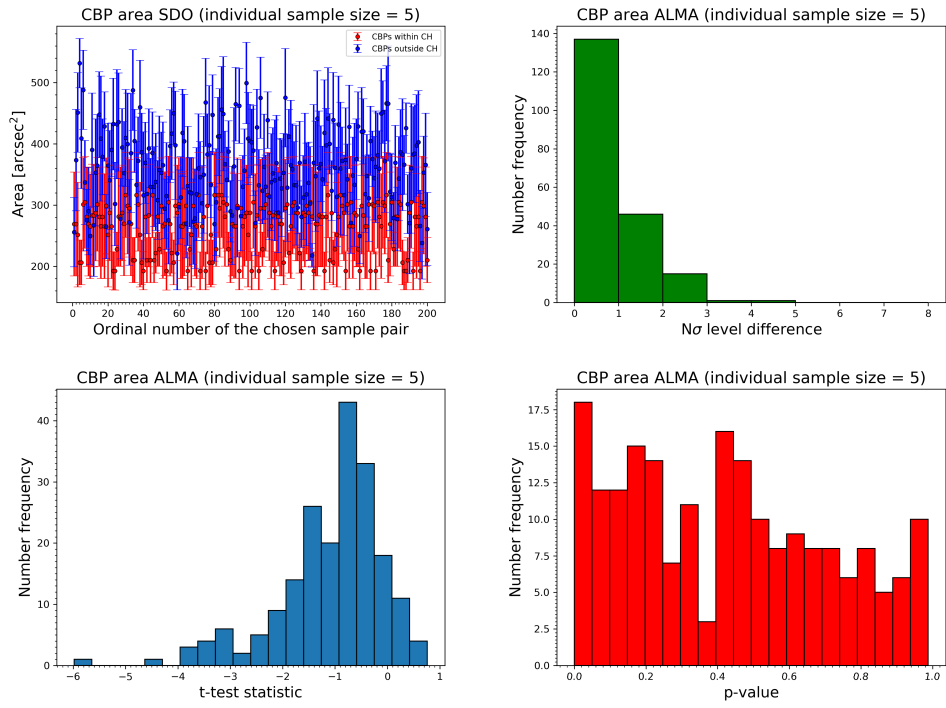


Fig. A.3. Same as Fig. A.1, but for the CBP area.

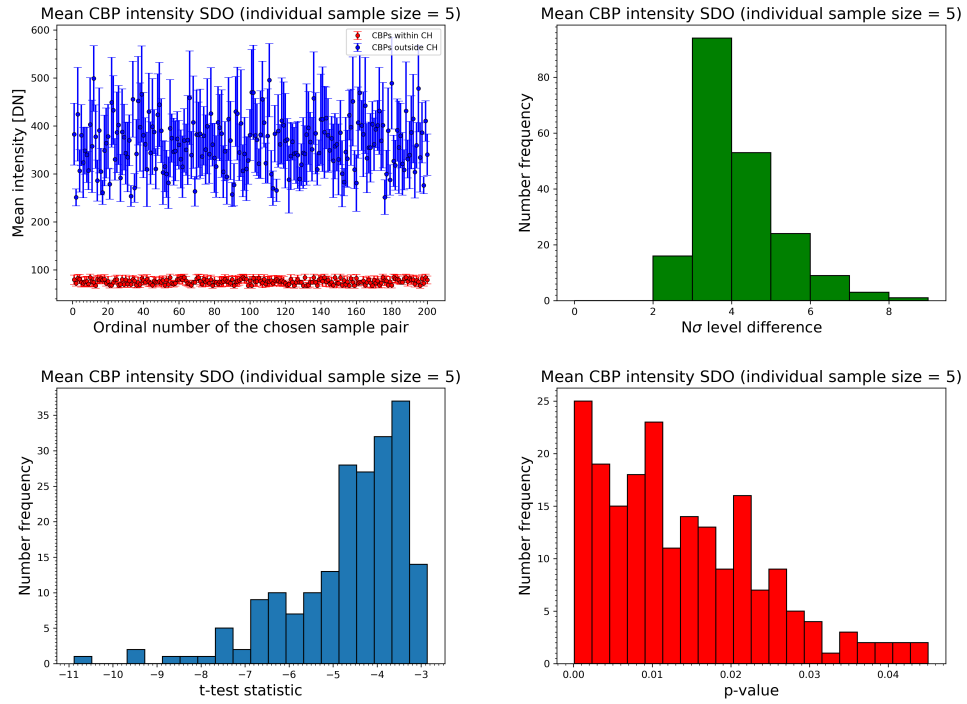


Fig. A.4. Same as Fig. A.1, but for SDO EUV data.

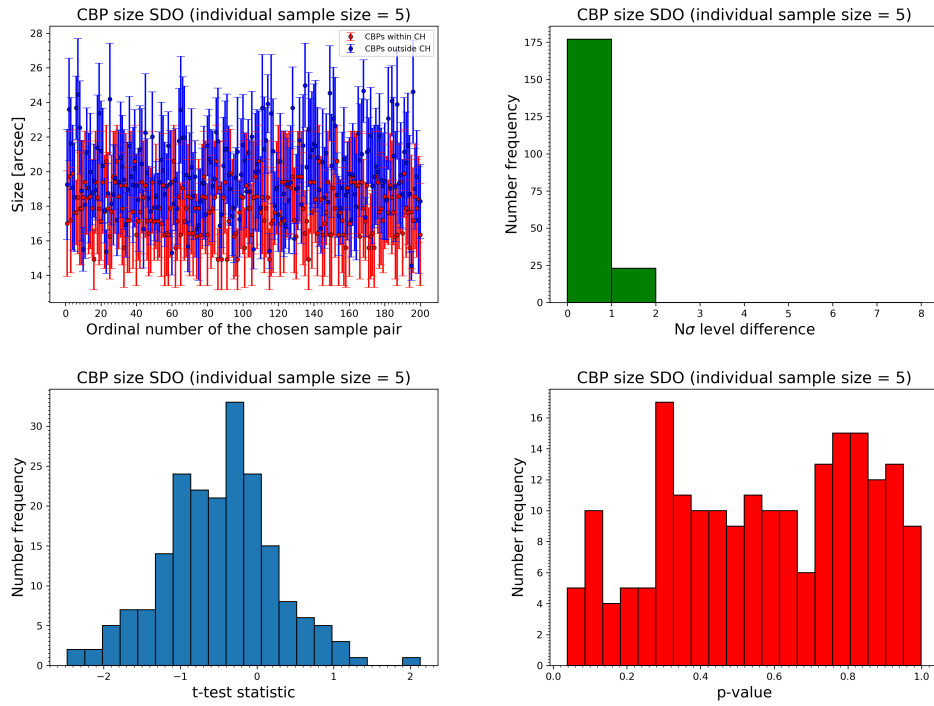


Fig. A.5. Same as Fig. A.1, but for the CBP size and SDO EUV data.

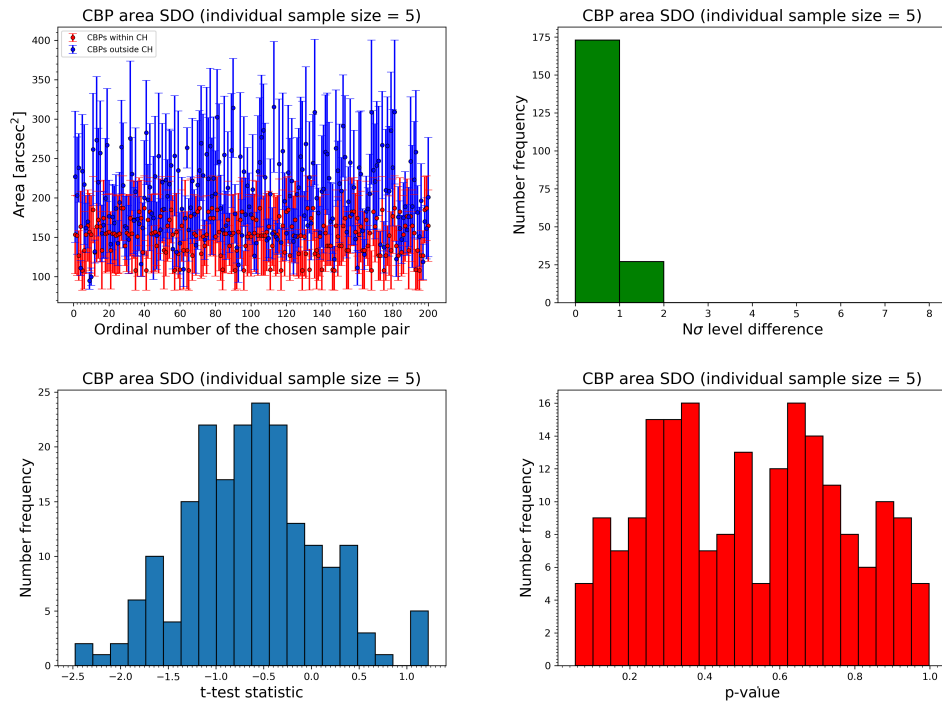
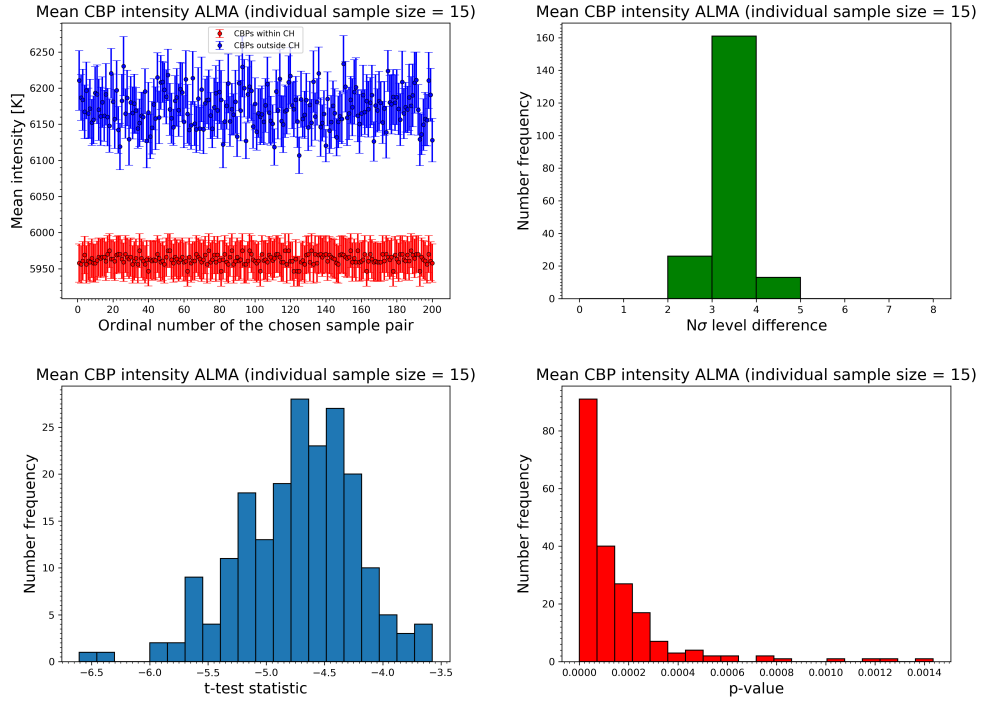
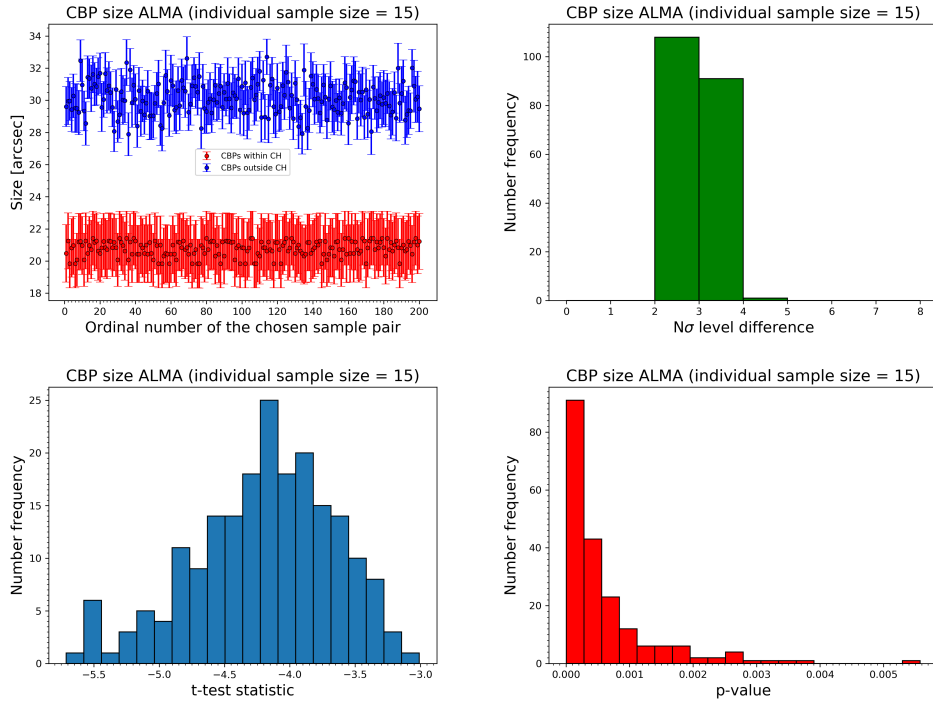


Fig. A.6. Same as Fig. A.1, but for the CBP area and SDO EUV data.

**Appendix B: Statistical analysis of the physical properties for CBPs within and outside CH3**



**Fig. B.1.** Same as Fig. A.1, but for the CH3, with individual CBP sample containing 15 CBPs.



**Fig. B.2.** Same as Fig. A.1, but for the CBP size and CH3, with individual CBP sample containing 15 CBPs.

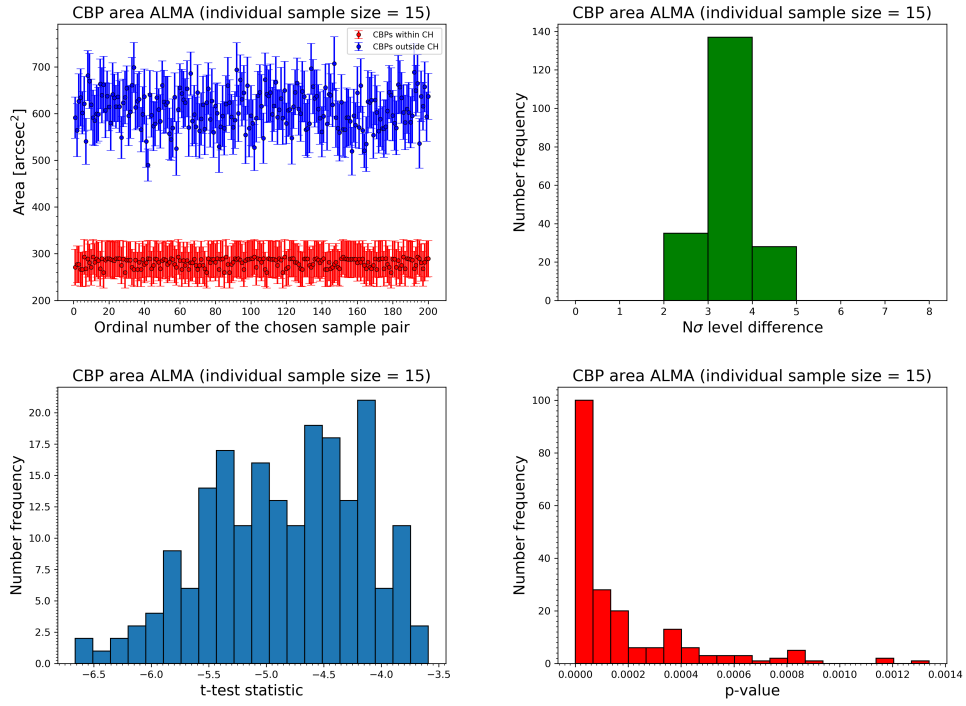


**Fig. B.3.** Same as Fig. A.1, but for the CBP area and CH3, with individual CBP sample containing 15 CBPs.

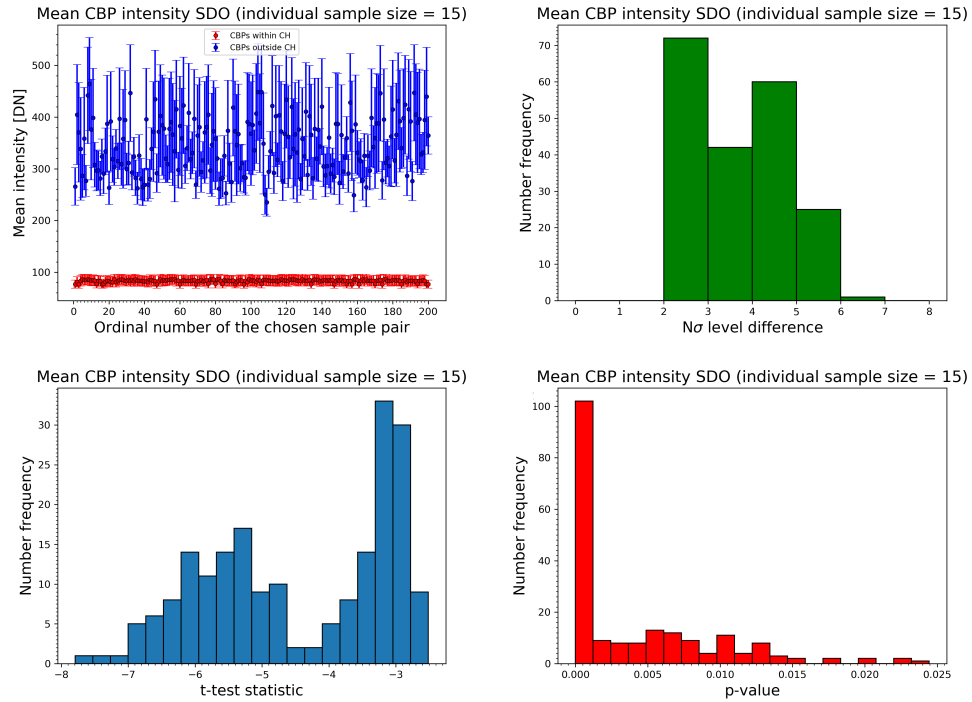


**Fig. B.4.** Same as Fig. A.1, but for SDO EUV data and CH3, with individual CBP sample containing 15 CBPs.

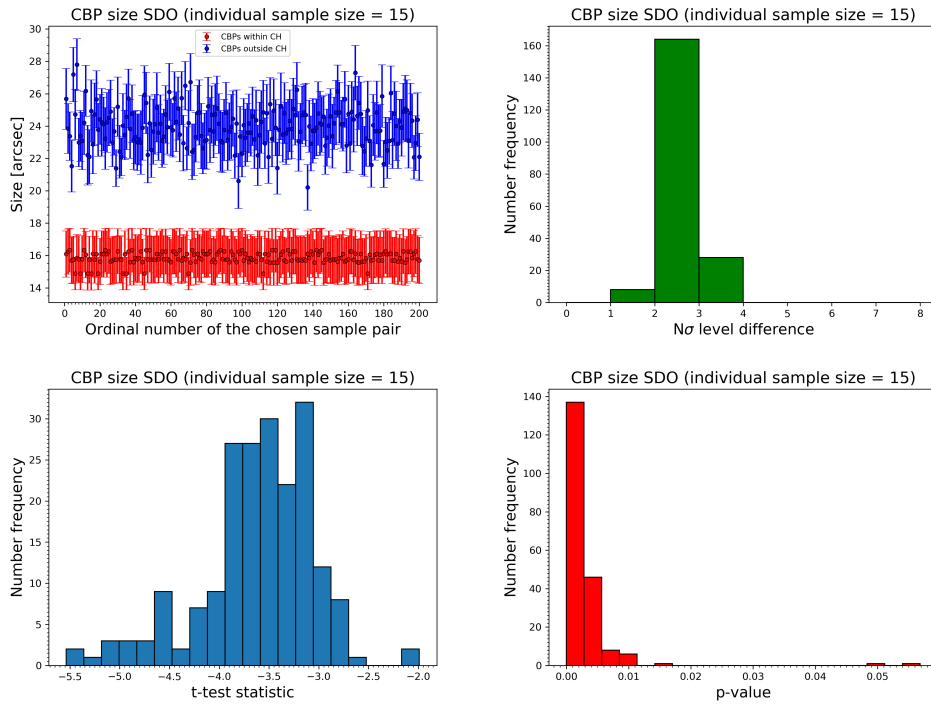


**Fig. B.5.** Same as Fig. A.1, but for the CBP size, SDO EUV data and CH3, with individual CBP sample containing 15 CBPs.

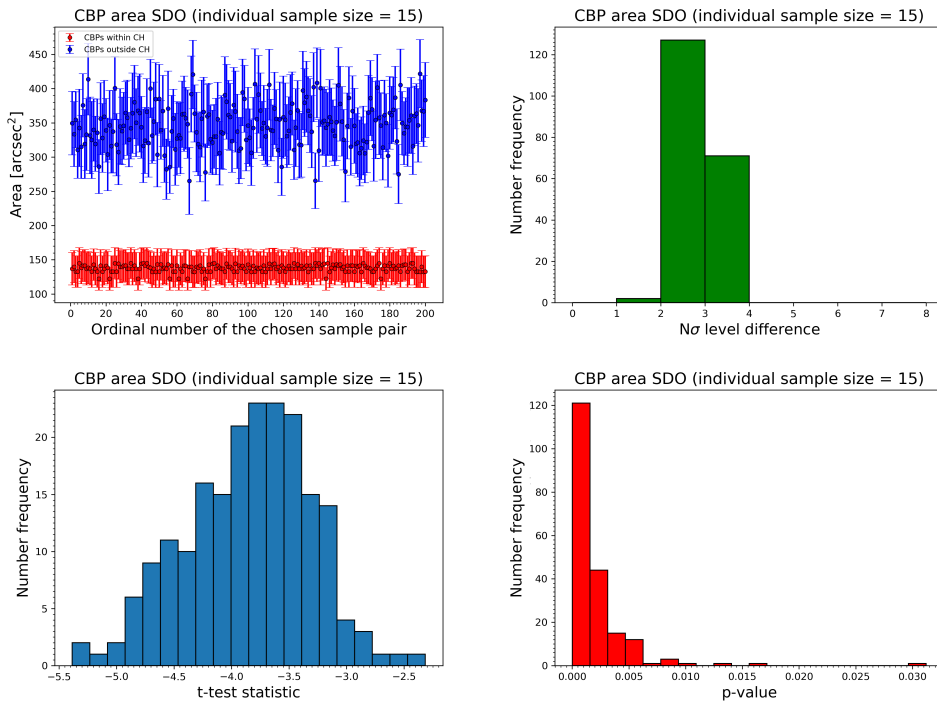


**Fig. B.6.** Same as Fig. A.1, but for the CBP area, SDO EUV data and CH3, with individual CBP sample containing 15 CBPs.

**Appendix C: Statistical analysis of the physical properties for CBPs within and outside CH4**

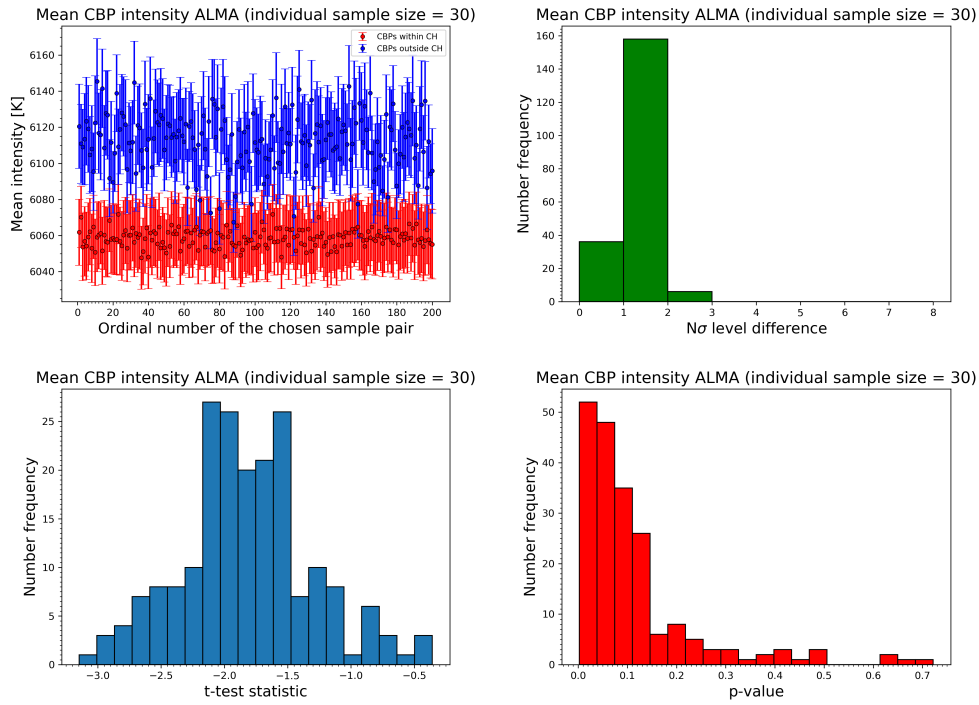


**Fig. C.1.** Same as Fig. A.1, but for the CH4, with individual CBP sample containing 30 CBPs.

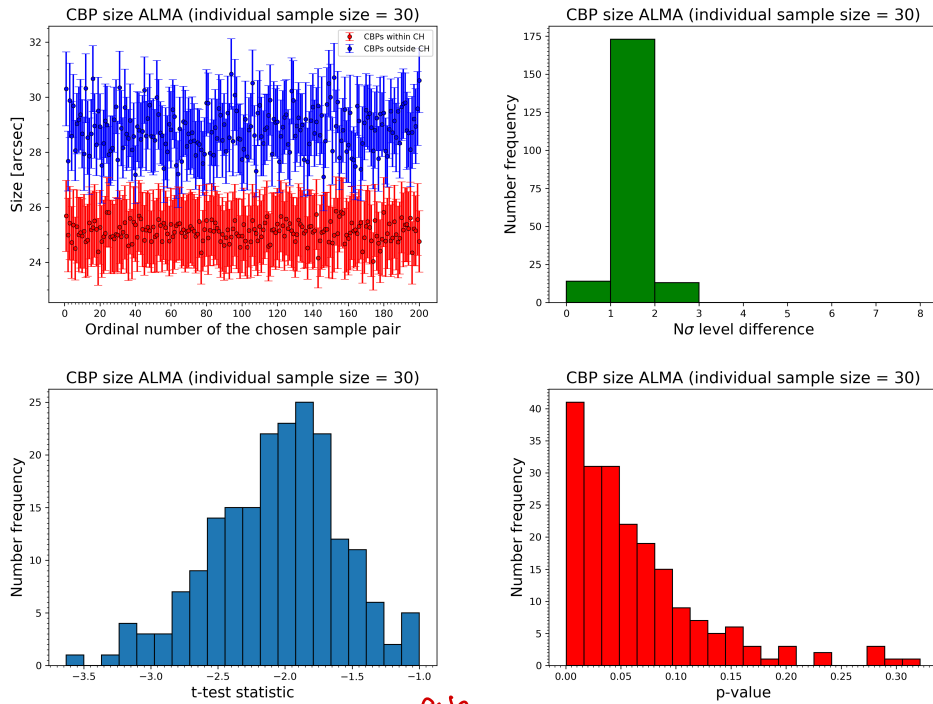


**Fig. C.2.** Same as Fig. A.1, but for the CBP size and CH4, with individual CBP sample containing 30 CBPs.

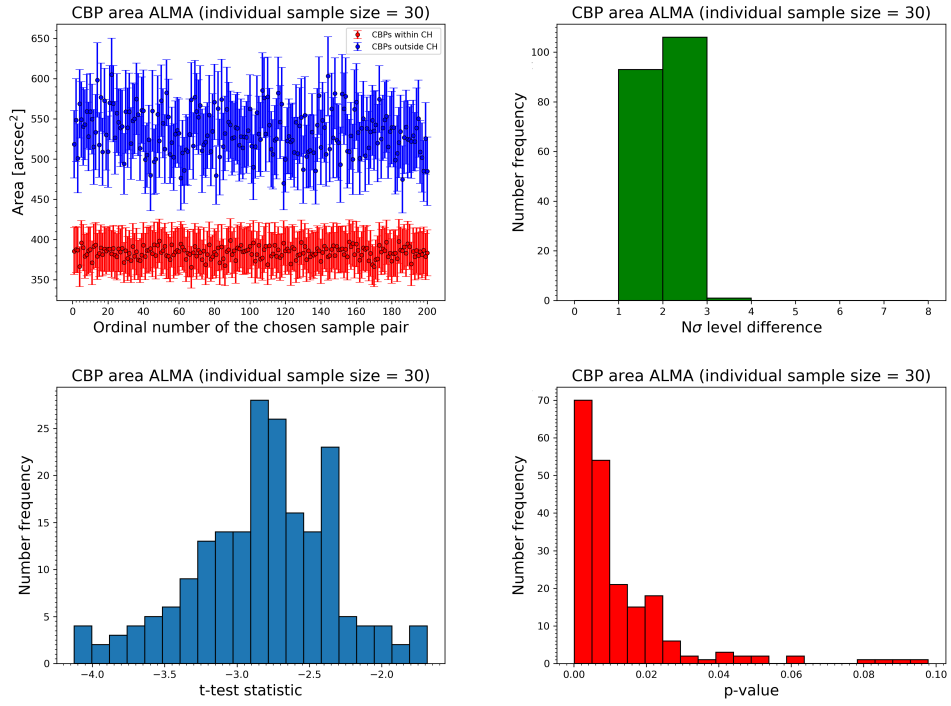


Fig. C.3. Same as Fig. A.1, but for the CBP area and CH4, with individual CBP sample containing 30 CBPs.

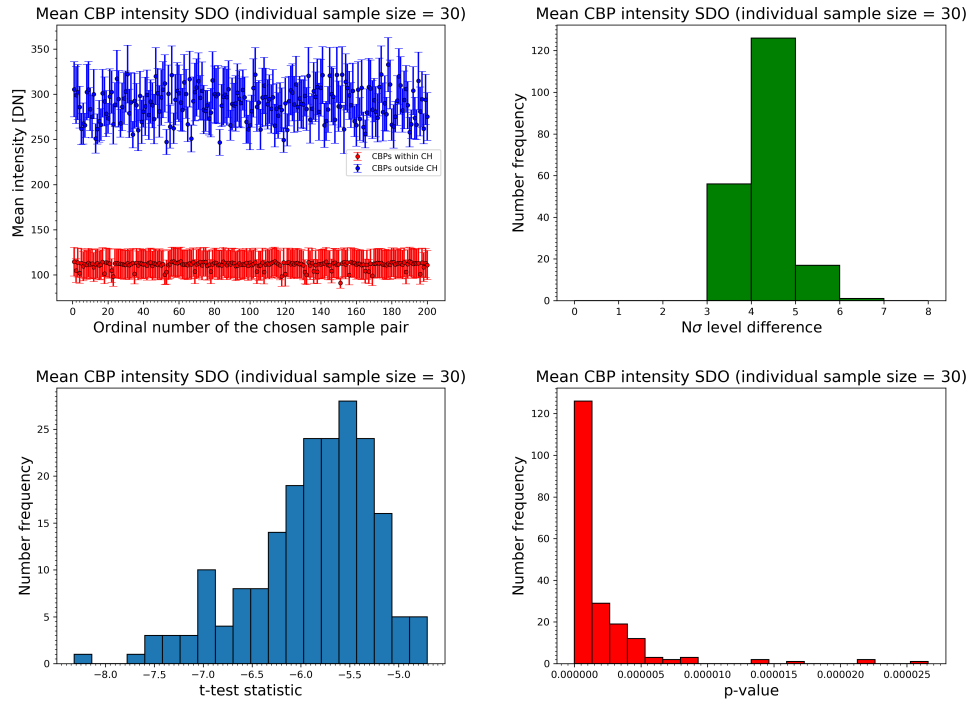


Fig. C.4. Same as Fig. A.1, but for SDO EUV data and CH4, with individual CBP sample containing 30 CBPs.

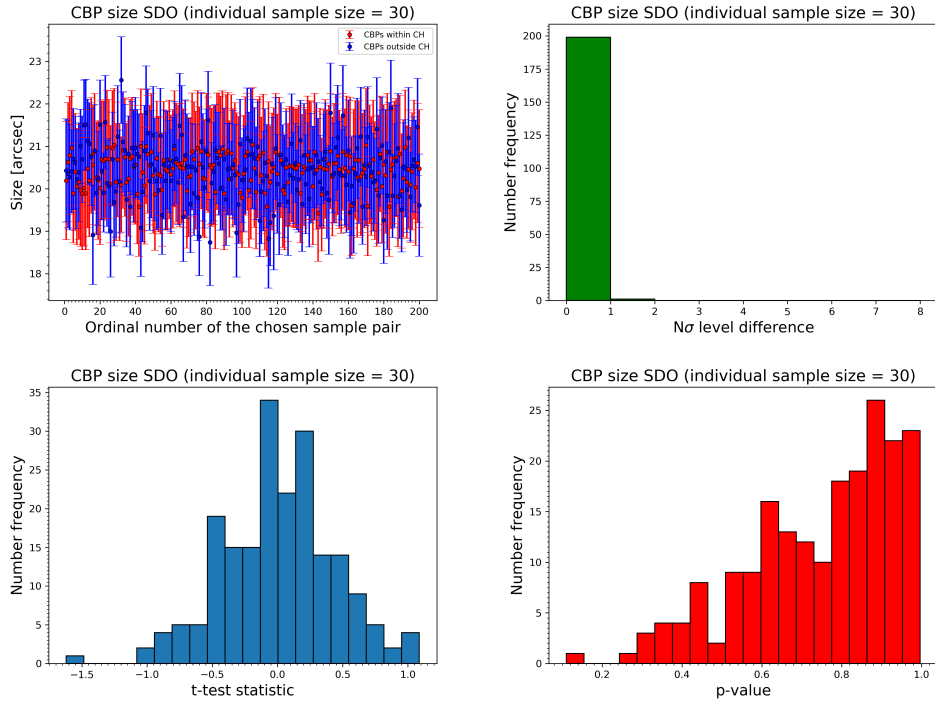


Fig. C.5. Same as Fig. A.1, but for the CBP size, SDO EUV data and CH4, with individual CBP sample containing 30 CBPs.

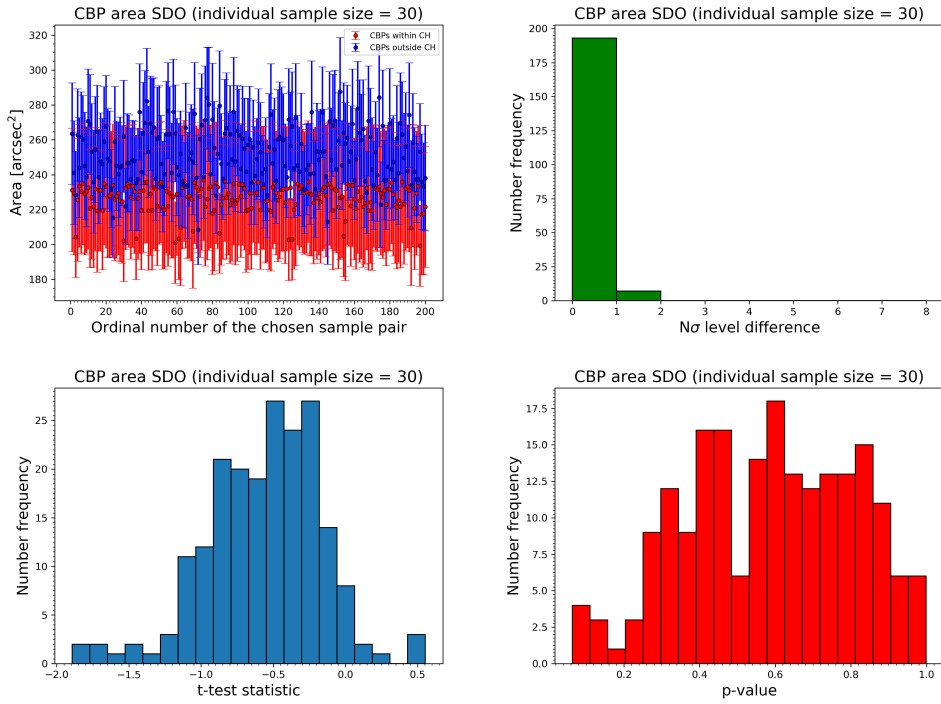


Fig. C.6. Same as Fig. A.1, but for the CBP area, SDO EUV data and CH4, with individual CBP sample containing 30 CBPs.

Appendix D: Statistical analysis of the physical properties for CBPs within and outside CH5

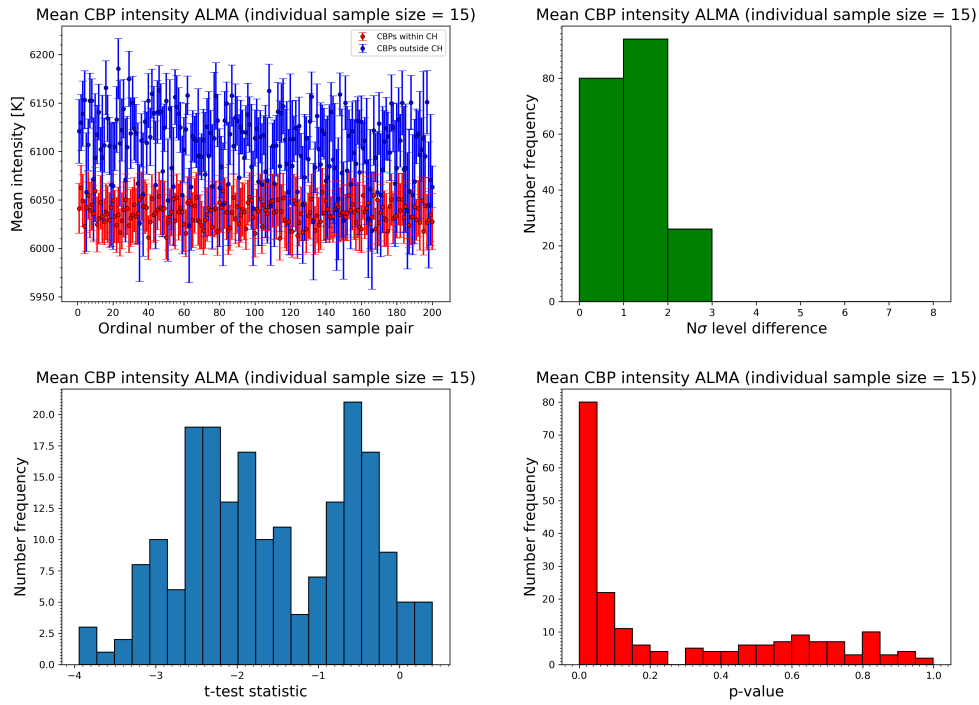


Fig. D.1. Same as Fig. A.1, but for the CH5, with individual CBP sample containing 15 CBPs.

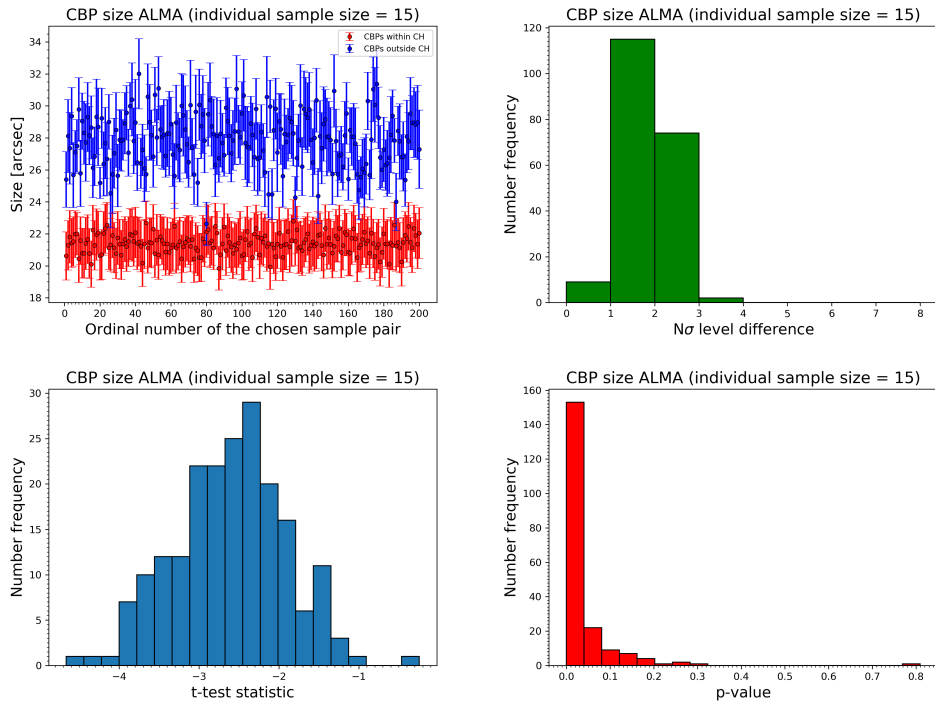
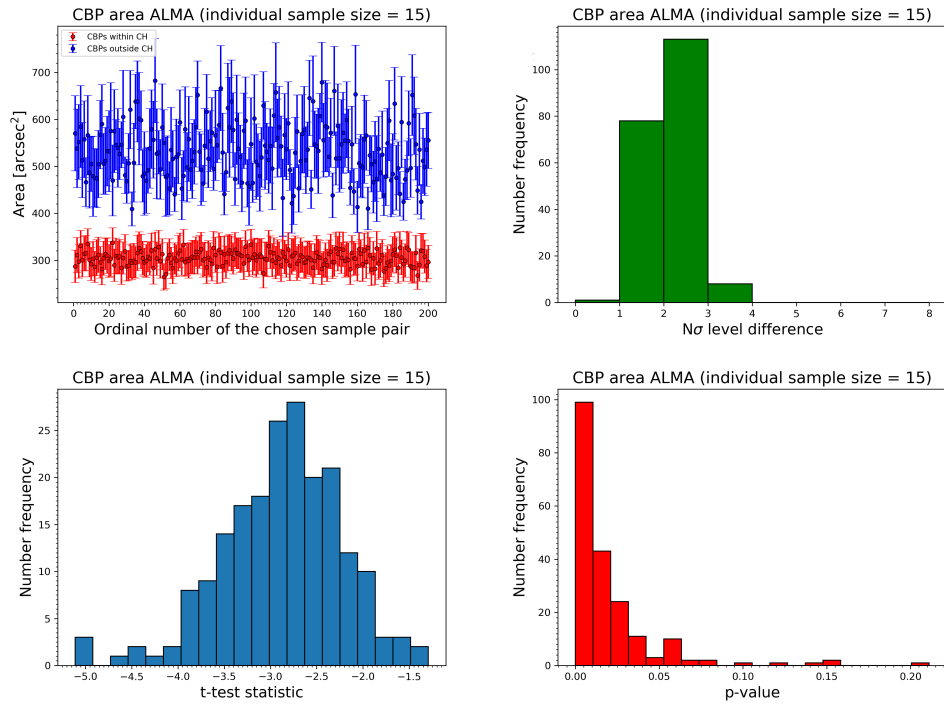
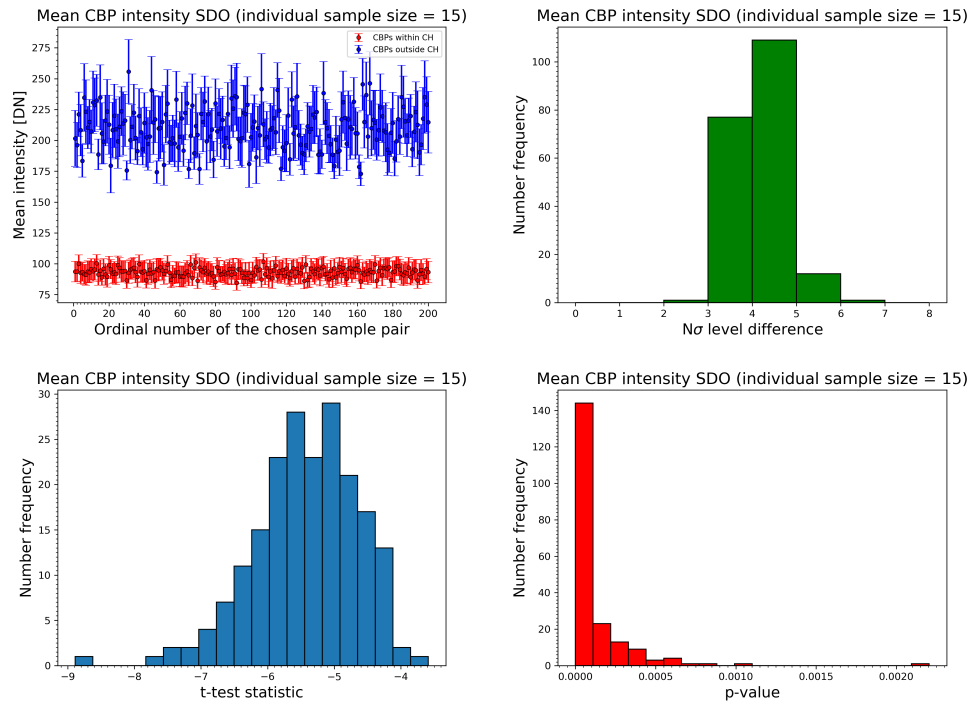


Fig. D.2. Same as Fig. A.1, but for the CBP size and CH5, with individual CBP sample containing 15 CBPs.



**Fig. D.3.** Same as Fig. A.1, but for the CBP area and CH5, with individual CBP sample containing 15 CBPs.



**Fig. D.4.** Same as Fig. A.1, but for SDO EUV data and CH5, with individual CBP sample containing 15 CBPs.

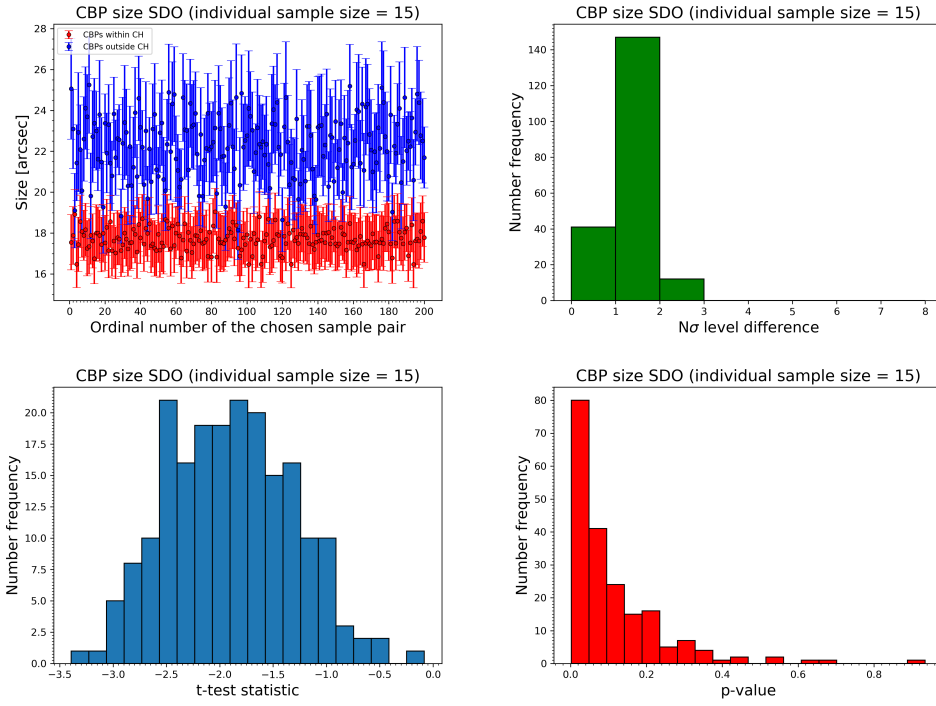


Fig. D.5. Same as Fig. A.1, but for the CBP size, SDO EUV data and CH5, with individual CBP sample containing 15 CBPs.

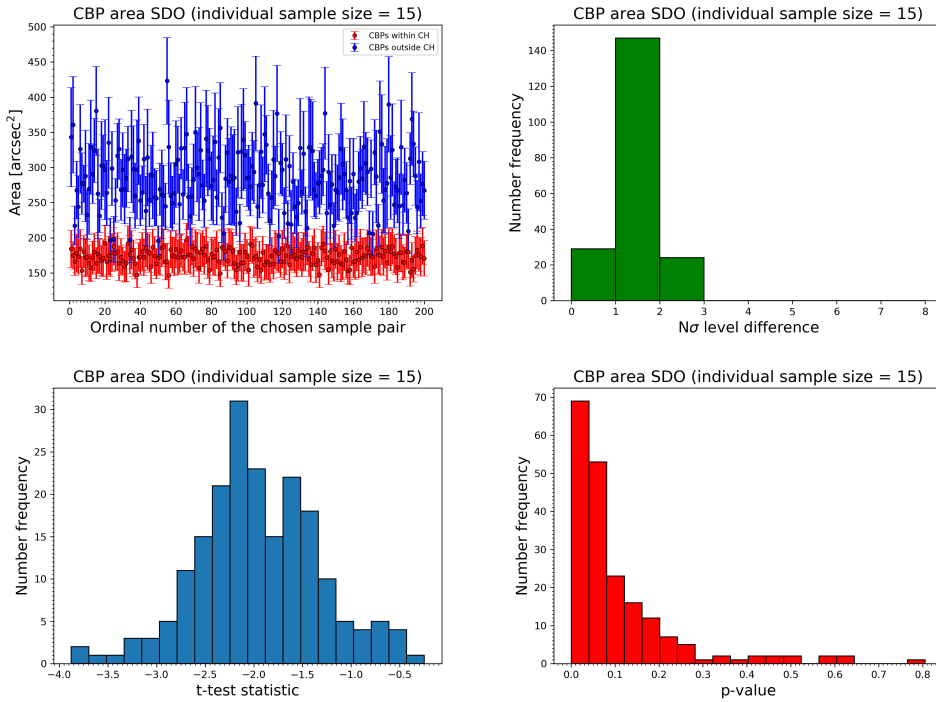


Fig. D.6. Same as Fig. A.1, but for the CBP area, SDO EUV data and CH5, with individual CBP sample containing 15 CBPs.